The Protein Disulfide Isomerase ERp57 Regulates the Steady-State Levels of the Prion Protein

Mauricio Torres[1,2#*], Danilo B. Medinas[1,2*], José Manuel Matamala[1,3], Ute Woehlbier[1,2], Víctor Hugo Cornejo[1,2], Tatiana Solda[4], Catherine Andreu[1,2], Pablo Rozas[1,2], Soledad Matus[1,5], Natalia Muñoz[1,5], Carmen Vergara[3], Luis Cartier[3], Claudio Soto[8], Maurizio Molinari[4,6,7], Claudio Hetz[1,2, 9].

[1]From Neuroscience Biomedical Institute, Faculty of Medicine, University of Chile, Santiago, Chile.
[2]Institute of Biomedical Sciences, Center for Molecular Studies of the Cell University of Chile, Santiago, Chile.
[3]Department of Neurological Sciences, Faculty of Medicine, University of Chile.
[4]Institute for Research in Biomedicine, Bellinzona, Switzerland.
[5]Neurounion Biomedical Foundation, CENPAR, Santiago, Chile.
[6]Università della svizzera italiana, Lugano, Switzerland
[7]Ecole Polytechnique Fédérale de Lausanne, School of Life Sciences, Lausanne, Switzerland
[8]Department of Neurology, University of Texas Medical School, Houston, USA.
[9]Harvard School of Public Health, Boston, USA.

Running title: *ERp57 controls PrP levels*

To whom correspondence should be addressed: Claudio Hetz, Independencia 1027, Faculty of Medicine, Institute of Biomedical Sciences, University of Chile, Santiago, Chile. P.O.Box 70086. Tel.: (56)2978-6506; website: www.hetzlab.cl. Email: chetz@med.uchile.cl and chetz@hsph.harvard.edu
Current address: Center for Biological Research in Patagonia, University of Magallanes, Coyhaique, Chile.
*co-first authors

Background: ERp57 is a disulfide isomerase upregulated in Prion related-disorders but its impact on PrP biology is unknown.
Results: ERp57 gain- and loss-of-function can respectively increase or reduce PrP levels in neurons, in cell culture and animal models.
Conclusion: ERp57 regulates steady-state prion protein levels.
Significance: ERp57 is a cellular factor involved in the folding and quality control of PrP, representing a novel therapeutic target in Prion-related diseases.

ABSTRACT

Although the accumulation of a misfolded and protease-resistant form of the prion protein (PrP) is a key event in Prion pathogenesis, the cellular factors involved in its folding and quality control are poorly understood. PrP is a glycosylated and disulfide-bonded protein synthesized at the endoplasmic reticulum (ER). The ER foldase ERp57 (also known as Grp58) is highly expressed in the brain of sporadic and infectious forms of Prion-related disorders. ERp57 is a disulfide isomerase involved in the folding of a subset of glycoproteins in the ER as part of the calnexin/calreticulin cycle. Here we show that levels of ERp57 increase mainly in neurons of Creutzfeldt-Jacob patients. Using gain- and loss-of-function approaches in cell culture we demonstrate that ERp57 expression directly controls the maturation and total levels of wild-type PrP and mutant forms associated with human disease. In addition, we found that PrP physically interacts with ERp57, and also with the closest family member PDIA1, but not ERp72. Furthermore, we generated a conditional knockout mouse for ERp57 in the nervous system and detected a reduction in the steady-state levels of the mono- and non-glycosylated forms of PrP in the brain. In contrast, ERp57 transgenic mice showed increased levels of endogenous PrP. Unexpectedly, ERp57 expression did not affect the susceptibility of cells to ER stress *in vitro* and *in vivo*. This study identifies ERp57 as a new modulator of PrP levels and may help understanding the consequences of ERp57 upregulation observed in human disease.

Prion-related disorders (PrDs) are fatal and rare neurodegenerative disorders characterized by

1

spongiform degeneration of the brain accompanied by the accumulation of a misfolded form of the prion protein (PrP) (1). PrDs can be classified as sporadic, familiar and infectious forms, affecting both humans and other mammals, where Creutzfeldt-Jacob disease (CJD) is the most frequent form in humans. The "protein-only" hypothesis postulates that the pathogenesis of infectious PrD forms involves a conformational change of wild-type PrP (here referred to as PrP^C) to a protease-resistant form (PrP^{RES}), initiated by a direct interaction between the two PrP forms (2). In infectious forms of the disease, PrP misfolding occurs mainly in the plasma membrane and in the endocytic pathway, whereas in familial forms the pathological changes in the conformation of PrP are proposed to occur during its synthesis at the endoplasmic reticulum (ER) (reviewed in (3)). Human PrP^C biosynthesis involves a series of post-translational modifications including the addition of N-linked glycosylations at Asn^{181} and Asn^{197}, the formation of a disulfide bridge between Cys^{179} and Cys^{214}, and the addition of a GPI anchor at Ser^{230}, among other post-translational modifications (1, 4). About 10% of PrP^C is not properly folded at the ER and is removed by the proteasome through the ER-associated degradation (ERAD) pathway (5, 6). Once folded, PrP^C is transported to the plasma membrane where it locates mainly to lipid raft microdomains via its GPI anchor (4, 7). Although PrP misfolding is the triggering step initiating PrDs, the cellular factors involved in the folding/misfolding of PrP are unknown.

Different reports have shown that the accumulation of misfolded PrP induces ER stress in infectious PrD forms (8–16), while in familial forms of PrDs the involvement of protein folding stress responses is less clear (17–19). ER stress triggers an adaptive reaction known as the unfolded protein response (UPR), which controls the expression of a diverse group of target genes involved in protein folding, quality control mechanisms and ERAD (20, 21). When these pro-survival mechanisms are unable to recover ER proteostasis, the UPR triggers apoptosis (22). ER stress has been proposed to have two main consequences on PrD progression, (i) it may contribute to the neurological impairment due to the repression of the synthesis of a cluster of synaptic proteins (11, 12), and (ii) it may operate as a signal to trigger neuronal loss (9). *In vitro* experiments have shown that a vicious cycle may operate in prion pathogenesis where prion misfolding predisposes cells to ER stress, which then may facilitate partial misfolding of PrP^C and, thus, prion replication (15,

23–26). Importantly, ER stress is also emerging as a driver of most common neurodegenerative diseases including Alzheimer´s disease, Parkinson and ALS (27).

A proteomic study of sporadic CJD brain tissue revealed that the major protein upregulated in this pathology is the ER foldase ERp57 (also known as Grp58 or PDIA3) (28). This observation was then confirmed in sporadic, but also new variant CJD cases, in addition to animal models of infectious PrD (8–10, 13, 14, 18, 23). ERp57 is a member of the protein disulfide isomerase (PDI) family, a group of around 21 proteins that catalyze the formation and isomerization of disulfide bonds thereby facilitating protein folding (29). Accumulating evidence support a functional role of PDIs in a variety of protein misfolding disorders affecting the nervous system (30). ERp57 is a central component of the calnexin (CNX) and calreticulin (CRT) cycle, involved in the folding and quality control of a subgroup of glycoproteins in the ER (31, 32). Although genetic ablation of ERp57 expression in mice is embryonically lethal (33, 34), *Erp57* deficient cells do not develop drastic alterations in the folding of glycosylated proteins and only a small subgroup of putative substrates are affected (35, 36). Beside its role in the CNX and CRT cycle, ERp57 is required as a scaffold protein for the assembly of the heavy chain of the MHC class I peptide loading complex, a function independent of its enzymatic activity involving covalent bonding with tapasin (37–39). Additional functions for ERp57 are reported, including the modulation of ER calcium homeostasis and STAT3 signaling (34, 40, 41). Although PDIs have been proposed to have neuroprotective activities (30), a drug screening identified a pro-apoptotic role of ERp57 and PDIA1 in models of neurodegeneration (42).

Only few studies have attempted to address the impact of ERp57 in PrDs. Using cell culture experiments we showed that ERp57 expression protects cells against the toxicity of infectious PrP forms (10). An interactome analysis indicated that PrP^C physically associates with ERp57, and pharmacological inhibition of PDI activity increased the levels of prion replication *in vitro* (10, 43). PrP^C also binds to CNX and CRT (44). Expression of PDIA1, the closest family member to ERp57, is also induced in PrD rodent models. PDIA1 expression has protective effects against mutant PrP associated with human disease, reducing ER stress levels (18). *In vitro* studies also suggested that disulfide bonds may contribute to PrP misfolding and aggregation (45–49).

Based on this evidence, here we investigate the possible impact of ERp57 in the expression of PrP using gain- and loss-of-function approaches both in cell culture models and genetically modified mice. Our results support an active involvement of ERp57 in the fine-tuning of the protein levels of PrP.

EXPERIMENTAL PROCEDURES
Human samples - The study was conducted according to the provisions of the Helsinki Declaration, and was designed in accordance with the relevant Chilean legislation and carried out with the approval of the Ethics Committee of the El Salvador Hospital, Santiago, Chile. Autopsies and human sample use were approved by the Ethics Committee of the Faculty of Medicine of University of Chile and by the FONDECYT funding agency (protocol number CBA #0323 FMUCH).

Histological analysis - For histological analysis of human tissue, 10 µm thick sections were obtained from formalin fixed, paraffin-embedded blocks of the brains of CJD and control patients. The paraffin-embedded sections were deparaffinized in xylene, followed by rehydration in a decreasing concentration of ethanol solutions. For routine pathological examination, deparaffinized sections from all blocks were stained with hematoxylin and eosin. Sections for immunohistochemistry (IHC) were incubated in 10 mM sodium citrate buffer (pH 6.0) and heated three times in a microwave oven for 5 min for antigen recovery, washed in TBS IHC wash buffer, treated with formic acid for 5 min, and washed again. Sections were then pretreated with 0.3% H_2O_2 in methanol for 30 min at room temperature to inhibit endogenous peroxidase activity. After washing twice with TBS IHC wash buffer for 5 min each, sections were blocked with 3% normal horse serum for 30 min at room temperature, followed by incubation with anti-ERp57 (1:100, Santa Cruz Biotechnology), anti-PDIA1 (1:100, Abcam), anti-ERp72 (1:100, Stressgen), anti-KDEL (1:100, Stressgen), and anti-PrP 6D11 (1:500, SIGNET) in a humidified chamber at 4° C overnight. Negative control sections were incubated with a negative control reagent (Dako) instead of primary antibodies. After washing twice with TBS IHC wash buffer for a total time of 5 min, the sections were incubated with the respective biotinylated secondary antibody for 30 min at room temperature, rinsed twice with TBS IHC wash buffer for a total of 5 min, followed by incubation with the avidin-biotin ABC kit (Vector Laboratories) for 30 min at room temperature. After rinsing with TBS IHC

wash buffer, peroxidase labeling was visualized with DAB (Impact DAB, Vector Laboratories) for 3 min at room temperature. Sections were then rinsed in tap water, dehydrated for 10 min, cleared and mounted.

For histological analysis of mouse tissue, animals were anesthetized using ketamine/xylazine and perfused intracardially with ice-cold saline followed by 4% paraformaldehyde (PFA) in PBS (pH 7.4). After 24 h post-fixation in 4% PFA, brains were cryoprotected in 30% sucrose in PBS. Twenty-five micrometer thick coronal brain sections were obtained using a Leica cryostat (Leica, Nussloch, Germany). Sections were pretreated with 3% H_2O_2 in methanol for 30 min at room temperature followed by incubation in citrate buffer (pH 6.0) for 15 min at 95 ºC for antigen recovery. After two washes in PBS for 5 min each, sections were blocked with 5% BSA, 0.3% Triton X-100 in PBS for 1 h at room temperature followed by incubation with anti-NeuN (1:300, Millipore) and anti-GFAP (1:250, Dako), or anti-ERp57 (1:100, Santa Cruz Biotechnology) in a humidified chamber at 4ºC overnight. After washing three times in PBS, sections were incubated with goat anti-mouse IgG Alexa Fluor 594 and goat anti-rabbit IgG Alexa Flour 488 (1:1000, Invitrogen) or HRP-conjugated goat anti-rabbit IgG (1:1000, Invitrogen) secondary antibodies for 1 h at room temperature. Immunohistochemistry was performed using DAB HRP substrate kit (Vector Laboratories) using manufacturer's instructions.

Cell culture, plasmids and cell transfections – Murine embryonic fibroblasts (MEFs), HEK293T, Neuro2a and NSC34 cells were cultured in DMEM supplemented with 10% fetal bovine serum and antibiotics (10,000 U/ml Penicillin, 10 µg/ml streptomycin), at 37°C and 5% CO_2. Transfections were performed using Effectene (Qiagen) according to manufacturer's instructions. Expression vectors of 3F4-tagged PrP mutants (PrP^{CTM}, PrP^{PG14}, PrP^{D177N} and PrP^{E199K}) and GFP fusion proteins were provided by David Harris (Washington University, USA) (50). The generation of PrP^C-3F4 and PrP^C-GFP constructs was previously described (26). The construct encoding GFP-tagged amyloid precursor protein (APP-GFP) was a gift from Patricia Burgos (Universidad Austral de Chile, Chile) (51). Plasmids to express PDIA1, ERp57 and ERp72 tagged with the V5 epitope were provided by Dr. Neil Bulleid (University of Glasgow, Scotland) (52). The KDEL-DsRED was obtained from Clontech Laboratories (Mountain View, CA, USA). Lentiviral expression vector pLKO.1 carrying shRNA against ERp57 (target

3

sequence 5'-GACCAGTTTATGTTTGTGGTT-3') or luciferase (for Mock control) were from The Broad Institute (Boston, MA, USA). Lentiviral particles were generated by standard methods and biosafety rules using HEK293T cells (53, 54). Stable knockdown of ERp57 (and Mock control) in Neuro2a cells was performed by lentiviral transduction of constructs encoding shRNA for ERp57 (or luciferase) followed by selection with puromycin. NSC34 cells stably expressing ERp57 were generated by transfection using Effectene (Qiagen) following the manufacturer's instructions. After 48 h of transfection, cells were selected using G418 (1.3 mg/ml).

SDS-PAGE and Western blot analysis – Cell culture pellets or brain tissue was homogenized on ice in RIPA buffer (20 mM Tris-HCl pH 8.0, 150 mM NaCl, 0.1% SDS, 0.5% DOC, 0.5% Triton X-100) containing a protease inhibitor cocktail (Roche, Basel, Switzerland). Protein concentrations were determined by micro-BCA assay (Pierce, Rockford, IL, USA). The equivalent of 30–50 µg of total protein was generally loaded onto 10% SDS-PAGE gels and analyzed by Western blot. The following antibodies and dilutions were used: anti-PrP (6D11) (1:5000, SIGNET), anti-PrP (3F4) (1:5000, Abcam), anti-ERp57 (1:2000, Santa Cruz Biotechnology), anti-PDIA1 (1:3000, Abcam), anti-ERO1Lα (1:2000, Novus Biologicals), anti-calnexin (1:2000, Stressgen), anti-BiP, (1:3000, Abcam), anti-β-Actin (1:2000, Cell Signaling), anti-Hsp90 (1:3000, Santa Cruz Biotechnology), and anti-V5 (1:5000, Invitrogen). After the incubation with the primary antibody, membranes were incubated for 1h at room temperature with HRP-conjugated secondary antibodies (all from Invitrogen). After washing, detection was performed by enhanced chemiluminescence assay (Amersham Biosciences, Cardiff, UK).

RNA extraction and quantitative real-time PCR - Total RNA from tissues was isolated using Trizol as recommended by the supplier (Life Technologies, 15596-018). The cDNA was synthesized with SuperScript III reverse transcriptase (Life Technologies, 11754250) using random primers p(dN)6 (Roche). Quantitative PCR reactions were performed using standard protocols (55). Actin mRNA was monitored as a housekeeping control. The following primers were used for *Erp57*: forward 5'-GAGGCTTGCCCCTGA-GTATG-3'and reverse 5'-GTTGGCAGTGCAATCC-ACC -3'. *Xbp1s*: forward 5'-TGCTGAGTCCGC-AGCAGGTG-3' and

reverse 5'-GACTAGCAGACT-CTGGGGAAG-3'. *Prp*: forward 5'-TCATCCCACGATCAGGAAGAT-3' and reverse 5'-TGCGTCACCCAGTACCAGAA-3'. *Edem*: forward 5'-AAGCCCTCTGGAACTTGCG-3' and reverse 5'-AACCCAATGGCCTGTCTGG-3'. *Bip*: forward 5'-TCATCGGACGCACTTGGAA-3' and reverse 5'-CAACCACCTTGAATGGCAAGA-3'. *Pdia1*: forward 5'-AGTT-CGCCCCAACCAGTACTT-3' and reverse 5'-CAAGATCAAGCCCCACCTGAT-3'. *Chop*: forward 5'-GTCCCTAGCTTGGCTGACAGA-3' and reverse 5'-TGGAGAGCGAGGGCTTTG'. *Actin*: forward 5'-CTCAGGAGGAGCAATGATCTTGAT-3' and reverse 5'-TACCACCATGTACCCAGGCA-3'. Splicing of XBP1 mRNA was also evaluated by conventional PCR using the primers *Xbp1*: forward 5'- ACACGCTTGGGAATGGACAC-3' and reverse 5'- CCATGGGAAGATGTTCTGGG-3', or by conventional PCR using the primers *Xbp1*: forward 5'-AAACAGAGTAGCAGCGCAGACTGC-3' and reverse 5'-GGATCTCTAAAACTAGAGGCTTGGTG-3' followed by digestion with the restriction enzyme PstI as described previously (56).

Proteinase K (PK), Filter-trap, and PNGase F experiments - PK assays were performed using a protocol previously described (26). Twenty micrograms of total protein in 1% NP40 buffer were treated for 30 min at 37°C with different concentrations of PK (2, 4 and 6 µg/ml). Proteolysis was stopped by adding phenylmethylsulfonyl fluoride followed by SDS-PAGE sample buffer; then heating the samples for 5 min at 95°C. For Filter-trap, 25 µg of total protein in 1% NP40 buffer was diluted in PBS containing 1% SDS to a final concentration of 0.25 µg/µl and filtered through cellulose acetate membrane with a pore size of 0.22 µm in a dot-blot apparatus (Bio-Rad, CA, USA). For loading control, 25 µg of total protein was analyzed by SDS-PAGE and Western blot or, in addition, diluted in PBS and loaded onto PVDF membrane in a dot-blot apparatus followed by Ponceau S staining. For deglycosylation assays, samples were treated with N-glycosidase F (PNGase F) (New England Biolabs) following manufacturer's recommendations. Briefly, samples were cooled to 25°C, and then the reaction buffer and 10 U of PNGase F were added. After 1 h at 37°C, SDS-PAGE sample buffer was added and samples were heated for 5 min at 95°C followed by electrophoresis. Finally, samples were analyzed by

Western blot using the anti-PrP (6D11) or (3F4) antibodies.

Pulse and chase experiments - Eighteen hours after transfection with expression vectors for 3F4-tagged PrP, MEFs were starved for 15 min in Met/Cys free medium, pulsed for 10 min with 50 µCi [^{35}S]Met/Cys in 1 ml starvation medium/dish, and chased for the indicated times with DMEM supplemented with 5 mM 'cold' Met/Cys. Post-nuclear supernatants (PNS) were prepared by solubilization of cells in 800 µl/dish ice-cold 2% CHAPS in HEPES-buffered saline (HBS), pH 6.8, containing 20 mM *N*-ethylmaleimide and protease inhibitors. CHAPS-insoluble material was separated by 10-min centrifugation at $10,000 \times g$. Immunoprecipitations were performed by adding protein A beads (Sigma; 1:10, w/v swollen in HBS) and the anti-PrP (3F4) antibody to the cleared extract followed by incubation for 2 h at 4°C. Immunoprecipitates were extensively washed three times with 0.5% CHAPS in HBS and resuspended in sample buffer for SDS-PAGE. Relevant bands were quantified using the ImageQuant software (Molecular Dynamics, Sunnyvale, CA). Gels were also exposed to BioMax films (Eastman-Kodak, Rochester, NY) and scanned with an AGFA scanner (Mortsel, Belgium).

Cycloheximide (CHX)-chase experiments were performed in MEFs transfected with PrP-GFP or APP-GFP constructs. Briefly, after 24 h of transfection cells were re-plated in a 48-well format and then 24 h later treated with 50 µg/ml of CHX for different time points. After the treatment, cells were detached by trypsinization and analyzed by flow cytometry.

Immunoprecipitations - HEK293T cells were transfected using Effectene transfection reagent. After 48 h, cells were collected and washed once in 1 ml of PBS pH 7.4. Subsequently, cells were resuspended in 500 µl of NP-40 buffer (0.2% NP-40, 50mM Tris-HCl pH7.5 , 150 mM NaCl) plus a protease inhibitor mix (Roche) and incubated overnight at 4 °C. Cell lysate was centrifuged at 10,000 rpm for 5 min at 4 °C. Subsequently, the supernatant was incubated with V5 antibody-coated agarose beads (V5 protein purification kit, MBL International) under constant agitation for 4 h at 4 °C. Then, the beads were washed 3 times with NP-40 buffer and the antibody-bound complexes were released by incubation with V5 peptide (MBL International) for 30 min at room temperature. Finally, the supernatant was obtained by centrifugation and analyzed by Western blot.

Generation of conditional ERp57 knockout mice - The ERp57 floxed mice were previously described where exons 2 and 3 were flanked with two *lox*P sites (33) and were kindly provided by Dr. Günther Hämmerling (German Cancer Research Center, Heidelberg, Germany). Mice expressing Cre recombinase under the control of the nestin promoter were obtained from The Jackson Laboratory (B6.Cg-Tg(Nes-cre)1Kln/J, 003771). To generate mice deficient in ERp57 in the central nervous system (CNS), ERp57 floxed animals were crossed with Nestin-Cre transgenic mice as we described before (8). Mice genotypes were designated as follows: ERp57[WT] (wild-type), ERp57[HET] (heterozygous, carrying one knockout allele), ERp57[KO] (conditional knockout). All experiments and animal care follow the Institutional Review Board´s Animal Care of the University of Chile (CBA # 0305 FMUCH). The following primers were used for genotyping of mice: *Erp57* floxed allele, forward 5'-CGCCAGCCTCTCCATTTAG -3'; *Erp57* floxed allele reverse 5'-CAGAGATCCTGCCTCTG -3', Cre forward 5'-GCGGTCTGGCAGTAAAAACTATC -3' and Cre reverse 5'-GTGAAACAGCATTGCTGT-CACTT -3'.

Generation of ERp57 transgenic mouse model – The transgenic mouse line overexpressing ERp57 was recently described (57) using the expression plasmid MoPrP.XhoI (58). In brief, the human ERp57 cDNA (Gene ID: 2923) was introduced into the plasmid using the XhoI restriction site. The resulting plasmid expressing the ERp57 sequence under the control of the PrP promoter was used to generate transgenic mice at the "Centro de Estudios Científicos" (CECS), Valdivia, Chile. The plasmid was purified and linearized for microinjection in mice with a FVB background. The primers used for genotyping were: forward 5'-AATTCCTGGATGCTGGGCAC-AAAC-3' and reverse 5'-TCTGCTTGTCATCGT-CGTCCTTGT-3'. Selected transgenic mouse lines were backcrossed into C57BL/6 background for more than 10 generations. All experiments and animal care followed the Institutional Review Board´s Animal Care of the University of Chile (CBA #0305 FMUCH).

Pharmacological induction of ER stress – For induction of ER stress *in vitro*, the ER stressors tunicamycin, thapsigargin, or brefeldin A were added to the cell culture medium followed by the measurement of ER stress markers by Western blot or

5

quantitative real-time PCR analysis as we previously reported (56, 59). The MTT method was employed to measure cell viability according to manufacturer's instructions (Promega). For induction of ER stress *in vivo*, mice received a single intraperitoneal injection of tunicamycin (5 mg/kg) diluted in sterile 150 mM glucose solution as described before (60). Control mice received intraperitoneal injection of vehicle (5% DMSO in 150 mM glucose solution). Mice were euthanized and tissue collected 24 h after injection.

Statistical analysis - For statistical analysis Graph Pad Prism Software Version 5.01 and SigmaPlot were used. All graphs show mean with SEM. Significance was calculated using Student's t-test or one-way or two-way ANOVA with Bonferroni post hoc test.

RESULTS

ERp57 levels are increased in neurons of CJD patients. Although it is reported that ERp57 levels are augmented in postmortem brain tissue derived from CJD patients (9, 28), the specific cell types responding have not been defined. To analyze the expression pattern of ERp57 in the brain, we performed immunohistochemistry studies. We confirmed the diagnosis of CJD patients by H&E staining and immunohistochemistry of PrP. The three subjects analyzed presented signs of spongiosis, neuronal loss, and gliosis (Fig. 1A and B). We then evaluated the expression pattern of ERp57 in the cerebellum using immunohistochemistry and found higher ERp57 levels in Purkinje cells of CJD patients compared to control subjects (Fig. 1C). We also monitored the expression levels of other ER chaperones in these patient samples. Analysis of PDIA1 distribution, the closest homologue to ERp57, also revealed to different extents an upregulation in CJD cases, whereas ERp72 did not show clear changes compared with control subjects (Fig. 1D). KDEL staining, which mostly recognizes BiP/Grp78 and Grp94, depicted a slight increase in some of the CJD cases analyzed with variable results. These results confirmed previous findings supporting the upregulation of ERp57 levels in postmortem brain tissue derived from CJD cases.

ERp57 deficiency reduces PrP levels. Since ERp57 selectively catalyzes the folding and disulfide bond formation of a subset of glycosylated proteins, we decided to analyze the expression levels of endogenous PrP^C in murine embryonic fibroblasts (MEFs) that are deficient for ERp57 (ERp57^{KO}) (36).

We observed a reduction in the steady-state levels of PrP^C in ERp57^{KO} cells when compared with wild-type control cells by Western blot analysis (Fig. 2A). Quantification of relative PrP^C levels in ERp57^{KO} MEFs indicated a reduction near 25% (Fig. 2A, right panel). To confirm these results in a different cell culture system, we knocked down ERp57 in Neuro2a cells after stable delivery of a shRNA construct using lentiviral vectors. A control shRNA against luciferase mRNA was employed (Mock). Targeting ERp57 resulted in significant reduction of PrP^C steady-state levels (Fig. 2B).

We then tested the effects of ERp57 deficiency on the levels of a mutant PrP form linked to CJD. We transiently transfected ERp57^{KO} and control MEFs with expression vectors for PrP^C or the murine PrP^{D177N} variant, equivalent to human mutation D178N linked to CJD, in addition to empty vector (Mock). All proteins contained the 3F4 tag to differentiate them from the endogenous protein. We then determined PrP levels using the anti-PrP 3F4 antibody and observed that ERp57 deficiency resulted in lower levels of both PrP forms (Fig. 2C). To corroborate these findings, ERp57^{KO} MEFs were transiently transfected with PrP-GFP fusion constructs (PrP^C-GFP and PrP^{D177N}-GFP) and the percentage of cells expressing GFP and the relative florescence intensity were quantified by flow cytometry analysis (Fig. 2D). Transfection of a GFP plasmid alone showed similar expression in both ERp57 WT and KO cells (Fig. 2D). Again, ERp57 deficiency significantly reduced the levels of wild-type and mutant PrP fused to GFP.

We then performed control experiments to determine if changes in PrP observed in ERp57^{KO} cells are due to a generalized deficit in protein folding in the ER. Thus, we overexpressed amyloid precursor protein (APP) fused to GFP (APP-GFP), another protein that traffics through the secretory pathway that undergoes glycosylation. We monitored the levels and distribution of APP using flow cytometry and fluorescent microscopy analysis and did not observe changes in APP-GFP levels or expression pattern when ERp57^{WT} and ERp57^{KO} MEFs were compared (Fig. 2E). These results suggest that ERp57 deficiency may affect client proteins, such as PrP, in a more specific manner.

Although mutant PrP forms associated with familial PrDs are retained at the ER, data linking their expression with the induction of an ER stress response is controversial (17–19). To study the impact of mutant PrP on ER physiology, we expressed in Neuro2a cells the murine PrP^{D177N} variant, PrP^{PG14}

6

(nine-octapeptide insertion) linked to Fatal Familial Insomnia (FFI), PrP[E199K] (equivalent to human PrP[E200K]) associated with familial CJD, and the point mutant L9R/3AV that generates an abnormal pathogenic form called PrP[CTM] (carboxy-terminal mutant) (61–63). All constructs contained the human PrP-3F4 epitope for detection (50) (Fig. 2F). These mutants were selected because of previous studies showing their partial retention at the ER and Golgi compartments (50, 64, 65). Unexpectedly, expression of all these mutant PrP forms did not trigger the upregulation of ERp57 at the protein (Fig. 2F, upper panel) or mRNA level (Fig. 2F, lower panel). Similarly, analysis of XBP1 mRNA splicing, a classical marker of ER stress (22), did not reveal any changes upon mutant PrP expression (Fig. 2G). We then tested whether mutant PrP overexpression could enhance the induction of ERp57 after treatment with the pharmacological ER stress agent thapsigargin. Again, the upregulation of *Erp57* or spliced *Xbp1* mRNA were not altered in Neuro2a cells expressing wild-type or mutant PrP (Fig. 2H). In summary, our results suggest that PrD-linked mutant PrP does not trigger the upregulation of ERp57 but under resting conditions ERp57 controls PrP steady-state levels.

ERp57 overexpression enhances PrP expression. We then performed gain-of-function studies by stably overexpressing a V5-tagged version of ERp57 (35) in the NSC34 neuronal cell line. First, we analyzed the expression levels of endogenous murine PrP[C] by Western blot. Consistent with our previous results, augmented steady-state levels of PrP[C] were observed in these cells when compared with control Mock cells (Fig. 3A). We then assessed the effects of ERp57-V5 overexpression on the levels of a set of PrP mutants linked to PrDs. We confirmed the altered localization of these PrP mutants using GFP fusion constructs together with the ER marker KDEL-dsRED, observing reduced expression at the plasma membrane and increased intracellular accumulation (Fig. 3B). We then transiently transfected PrP-3F4 constructs in NSC34 cells stably overexpressing ERp57-V5 and determined the relative expression levels of PrP after 48 h using Western blot analysis. In agreement with our loss-of-function experiments, overexpression of ERp57 increased the levels of PrP[C] and the mutants D177N, PG14, and E199K (Fig. 3C). ERp57 had only a slight effect on PrP[CTM], which had low expression levels. We then evaluated the misfolding of PrP in these experiments by treating protein extracts with different concentrations of proteinase K (PK). Consistent with increased levels of PrP upon ERp57-

V5 overexpression, the relative amount of PK-resistant forms of PrP was also augmented under these conditions (Fig. 3D). These observations indicate that ERp57 expression modulates steady-state levels of PrP wild-type and mutant forms in different cell culture models.

ERp57 deficiency alters PrP maturation. Based on the observation that ERp57 controls the expression of PrP at basal levels, we decided to monitor in detail its synthesis and maturation in ERp57[KO] cells. We performed pulse-chase experiments in ERp57[KO] and wild-type MEFs transiently transfected with 3F4-tagged PrP[C]. In control ERp57[WT] cells, the classical pattern of PrP maturation was observed over time, where non-glycosylated, mono-glycosylated and di-glycosylated PrP bands were visualized, in addition to PrP species with higher molecular weight showing more complex glycosylations (Fig. 4A, left panel). The nature of these bands was confirmed after the treatment of protein extracts with PNGase to deglycosylate PrP (Fig. 4B). We then studied the synthesis and maturation of PrP[C] in ERp57-deficient cells between 10 and 180 min after radioactive pulse (Fig. 4A, right panel). Under these conditions, we found a nearly 50% reduction in the average half-life of total overexpressed PrP[C] in ERp57-deficient cells (Fig. 4A). Importantly, no differences in the rate of PrP synthesis were found between ERp57[KO] and control cells as measured by the PrP-radioactive signal when we started the chase (t = 0-10 min) (Fig. 4A). Surprisingly, the band pattern of PrP in SDS-PAGE analysis performed without the reducing agent DTT in the sample buffer remained the same, suggesting the absence of an altered oligomerization into S-S linked assemblies in ERp57 deficient cells (Fig. 4A, lower panels), which is in contrast to the results reported for some ERp57 substrates (36).

To further assess whether PrP forms protein aggregates undetectable by Western blot, we carried out filter-trap analysis to evaluate the presence of large species that are retained in the 0.22-µm pores of the cellulose acetate membrane. Remarkably, we observed that ERp57-deficiency in MEFs promote the aggregation of endogenous PrP at basal levels (Fig. 4C). More over these large aggregates were susceptible to DTT treatment, suggesting disulfide-dependent interactions (Fig. 4D). Together these results suggest that a reduced folding efficiency of PrP in ERp57[KO] cells that leads to aberrant intermolecular disulfide bonds in the protein.

We then complemented these experiments by monitoring the steady-state levels of PrP[C]-GFP by

7

flow cytometry analysis in cells treated with cycloheximide to inhibit protein synthesis. Again, a lower stability of PrP^C was confirmed in ERp57^{KO} MEFs when compared to control cells (Fig. 4E, upper panel). In contrast, APP-GFP showed similar stability in both cell lines under the same experimental conditions (Fig. 4E, lower panel). Taken together, these results suggest that ERp57 may participate in the folding or the maturation of PrP^C.

ERp57 forms a protein complex with PrP. Based on our results showing that ERp57 modulates PrP^C levels and affects its maturation, we then investigated the possible physical interaction between PrP^C and ERp57. We co-transfected a PrP^C-3F4 construct together with a V5-tagged version of ERp57 in HEK cells. After 48 h, we immunoprecipitated ERp57-V5 and analyzed the possible association with PrP^C using Western blot analysis. We observed an interaction between ERp57-V5 and PrP^C-3F4, where the mono- and di-glycosylated forms of PrP were preferentially co-immunoprecipitated (Fig. 5A). As control, we then analyzed the possible association of PrP with V5-tagged PDIA1 or ERp72, two structurally related proteins to ERp57 (29). Immunoprecipitation of PrP^C-3F4 revealed only an interaction with PDIA1, but not with ERp72 (Fig. 5A). We then performed similar experiments with the PrP^{D177N} mutant. We detected an association between PrP^{D177N} and ERp57-V5 with a similar efficiency of co-immunoprecipitation as PrP^C (Fig. 5B). However, the di-glycosylated form of PrP^{D177N} was enriched in these experiments (Fig. 5B). These results suggest that ERp57 and PDIA1 form protein complexes with PrP.

ERp57 expression does not influence the susceptibility of cells to ER stress. Our results together with previous reports suggest that ERp57 may have a dual activity on PrDs, modulating PrP synthesis and the survival of cells under the ER stress reaction generated in the disease. Thus, we decided to monitor the impact of ERp57 expression on the susceptibility of cells to experimental ER stress. ERp57^{KO} and control MEFs were treated with the ER stress agent tunicamycin (Tm) for 16 h and the expression levels of different ER folding components were monitored, including ERp57, PDIA1, CNX, ERO1Lα, and BiP. No clear changes were observed between genotypes at basal levels or in cells undergoing ER stress (Fig. 6A), suggesting the lack of clear compensatory changes upon *Erp57* deletion. In agreement with these results, analysis of cell viability in cells treated with three different ER stress agents

indicated no differential vulnerability of ERp57-deficient cells (Fig. 6B).

We then performed similar experiments in NSC34 cells overexpressing ERp57-V5. Overexpression of ERp57 did not reduce the activation of XBP1 mRNA splicing or the upregulation of the ER stress pro-apoptotic factor *Chop* in cells treated with tunicamycin (Fig. 6C). Consistent with these results, no changes on the levels of a panel of ER folding factors was observed in ERp57-V5 overexpressing cells at basal levels or after treatment with tunicamycin (Fig. 6D). Finally, these cells did not shown any protection against ER stress when cell viability was monitored with the MTT assay after treatment with tunicamycin or thapsigargin (Fig. 6E). In summary, our results indicate that ERp57 expression does not influence the global response to ER stress, but it has a specific effect on controlling the levels of PrP.

The PrP expression pattern is altered in the brain of a conditional ERp57 knockout mouse. Although ERp57 deficiency in mice is embryonic lethal, a viable conditional B cell-specific knockout mouse was described before (33). We generated a CNS-specific ERp57 knockout mouse by crossing that floxed animal with a Cre transgenic mouse under the control of the *Nestin* promoter (Woehlbier and Hetz, unpublished). Targeting *Erp57* in the nervous system bypassed embryonic lethality since we were able to generate ERp57 heterozygous (ERp57^{HET}) and conditional knockout mice (ERp57^{cKO}). We confirmed the reduction of *Erp57* expression in both genotypes at the mRNA level using real-time PCR with a near 50% reduction in ERp57^{HET} animals and a complete loss of ERp57 mRNA expression in ERp57^{cKO} mice (Fig. 7A). These results were then validated in brain cortex, hippocampus and cerebellum using Western blot analysis (Fig. 7B).

Next, we evaluated mRNA levels of PrP in brain cortex of ERp57-deficient mice (Fig. 7C). Despite the slight induction observed in ERp57^{HET} animals, deficiency of ERp57 in the nervous system had no major impact on transcription of PrP (Fig. 7C). Then, the protein pattern of endogenous PrP was evaluated in the brain of ERp57-deficient mice (Fig. 7D). Quantification of different PrP species revealed a significant reduction of the mono-glycosylated PrP form in the cortex of ERp57^{cKO} mice (Fig. 7E, middle panel). We also found a small change in the levels of the non-glycosylated PrP form (Fig. 7E, right panel), whereas no differences in the levels of the di-glycosylated form were detected (Fig. 7E, left panel).

8

To assess whether targeting ERp57 in the brain alters ER proteostasis, we monitored the mRNA levels of a few ER stress-responsive genes including *Bip*, *Edem1*, *Pdi* and *Chop*. Overall no changes where observed when the three genotypes were compared using cerebellar extracts (Fig. 7F). Similarly, analysis of the expression levels of CNX, ERO1Lα, and BiP did not reveal any upregulation in ERp57-deficient animals (Figure 7G). Qualitative immunofluorescence analysis indicated that ERP57[cKO] mice do not show evident signs of neuronal loss or astrogliosis in CNS tissue (Fig. 7H). In summary, this data indicate that ERp57 deficiency in the nervous system impacts the steady-state levels of PrP expression *in vivo*.

Overexpression of ERp57 in neurons increases PrP expression in vivo. We recently generated a transgenic mouse that overexpresses a FLAG-tagged version of human ERp57 under the control of the PrP promoter (ERp57-Tg) (57). The overexpression of ERp57-FLAG in transgenic mice was confirmed in the cerebellum using Western blot analysis, observing a near 1.5 fold increase in ERp57 levels compared with non-transgenic littermates (Non-Tg) (Fig. 8A). The overexpression of ERp57 was also confirmed by immunohistochemistry (Fig. 8B). We then monitored PrP levels in these brain extracts. Remarkably, a significant increase in the total levels of PrP was observed in the cerebellum of 2-month-old ERp57-FLAG transgenic mice (Fig. 8C), whereas the mRNA levels of PrP were not altered (Fig. 8D).

We then monitored the susceptibility of ERp57-FLAG overexpressing mice to ER stress. We intraperitoneally injected these animals with the ER stress agent tunicamycin and then measured the levels of the ER stress markers *Chop* and spliced XBP1 mRNA in the brain using real-time PCR. Consistent with our *in vitro* experiments, ERp57 overexpression did not alter the susceptibility of cells to undergo ER stress (Fig. 8E). Taken together, these results suggest that enforced expression of ERp57 in the brain augments PrP levels.

DISCUSSION

An increase in the levels of ERp57 has been described in diseases such as Alzheimer's disease, amyotrophic lateral sclerosis, Parkinson's disease, Huntington's disease and PrD, among other pathologies (reviewed in (30)), although its biological significance has remained elusive. The induction of ERp57 has been associated with an UPR response due to the accumulation of misfolded proteins inside the ER, assisting in the folding and quality control of glycoproteins as part of the CNX/CRT cycle. Here we investigated the impact of ERp57 on PrP biogenesis. First, we confirmed the increased levels of ERp57 in patients diagnosed with sporadic CJD and identified a specific response in neurons. Since PrP is a disulfide bond-containing glycoprotein, we hypothesized that ERp57 could directly participate in the biosynthesis of PrP. Our results show that ERp57 deficiency alters the maturation and decreases the levels of both endogenous and exogenous PrP[C], while ERp57 overexpression has the opposite effect. In addition, similar results were obtained when a panel of disease-related PrP mutants was expressed, suggesting that PrP[C] and PrP mutant forms are possible clients of the ERp57-folding pathway. In agreement with this idea, we also established that both PrP[C] and PrP[D177N] physically interact with ERp57. Furthermore, we confirmed that PrP[C] also associates with PDIA1, but not with ERp72. On the other hand, it may be feasible that ERp57 and PDIA1 act on different conformational pools of unfolded/misfolded PrP, since PDIA1 is also part of the ERAD pathway (66) and may therefore target unfolded/misfolded PrP towards degradation. Of note, a recent report suggested that calnexin mediates a novel PrP clearance pathway under ER stress termed 'rapid ER stress-induced export' (RESET) (67). RESET involves the export of misfolded GPI proteins to the plasma membrane for subsequent degradation by the lysosome. It may be interesting to explore in the future if ERp57 also modulates the degradation of PrP by RESET.

To investigate the significance of ERp57 on the biology of PrP *in vivo*, we first generated a CNS-specific ERp57 knockout mouse model. Homozygous mice showed a near full loss of ERp57 in the CNS, whereas heterozygous animals showed a 50% reduction in ERp57 mRNA and protein levels. ERp57-deficient animals did not show major changes in the levels of the di-glycosylated PrP at steady state; however, we confirmed the reduction of the mono- and non-glycosylated form of endogenous PrP in ERp57 knockout animals. This may be explained by the compensatory mechanisms involving CNX and CRT. Another possibility is the functional replacement of ERp57 by other PDIs in neurons *in vivo*, including PDIA1. Furthermore, we have examined PrP levels in transgenic mice overexpressing ERp57 under the control of the prion promoter. We have recently reported a functional characterization of this transgenic line showing that overexpression of ERp57 improves recovery in peripheral nerve regeneration after mechanical injury

9

to sciatic nerve (57), indicating that the overexpressed chaperone is functional in the nervous system. Interestingly, PrP expression is induced in models of peripheral nerve degeneration (68), and its deficiency triggers myelin defects (69). Since mice overexpressing ERp57 displayed augmented levels of PrP in the nervous system, it remains to be determined if part of the beneficial effects of overexpressing ERp57 are due to enhancement of PrP expression.

Although ERp57 and PDIA1 have been suggested to protect cells against ER stress (70) due to its crucial role in assisting the folding of glycosylated proteins, we did not find evidence supporting a major role of ERp57 in the susceptibility of cells to ER stress and cell death *in vitro* and *in vivo* using multiple experimental systems. These observations may be explained by the fact that ERp57 may only catalyze the folding of a small subset of glycosylated proteins

in the secretory pathway (34–36). The expression of other PDI family members may maintain the global homeostasis of disulfide bond formation at the ER in neurons lacking ERp57 expression. Unexpectedly, we did not observe drastic compensatory changes in other PDIs or ER foldases when ERp57 expression was targeted, which again support the concept that ERp57 may assist the folding of a small subset of ER clients proteins and its deficiency does not cause a general perturbation of redox folding in the ER.

In future experiments, we plan to investigate if ERp57 modulates the progression of prion disease in infectious and genetic models of PrD. Overall, this study identifies a new component regulating PrP levels that may have relevance to understand the contribution of the cellular context during prion pathogenesis.

ACKNOWLEDGMENTS

CONFLICT OF INTEREST

The authors declare that they have no conflicts of interest with the contents of this article.

AUTHOR CONTRIBUTIONS

MT designed the study and experiments, performed experiments, analyzed data, and wrote the paper. DBM designed experiments, performed experiments, analyzed data, and wrote the paper. JMM designed experiments, performed experiments, and analyzed data. UW designed experiments, performed experiments, analyzed data, and wrote the paper. VHC performed experiments and analyzed data. TS performed experiments and analyzed data. CA performed experiments and analyzed data. PR performed experiments and analyzed data. SM performed experiments and analyzed data. NM performed experiments and analyzed data. CV performed experiments and analyzed data. LC designed experiments and analyzed the data. CS designed experiments and analyzed the data. MM designed experiments and analyzed the data. CH designed the study and experiments, analyzed the data, and wrote the paper. All authors have read and approved the final version of the manuscript.

REFERENCES

1. Prusiner, S. B. (1998) Prions. *Proc. Natl. Acad. Sci. U. S. A.* **95**, 13363–13383
2. Soto, C. (2011) Prion hypothesis: The end of the controversy? *Trends Biochem. Sci.* **36**, 151–158
3. Hetz, C. A., and Soto, C. (2006) Stressing out the ER: a role of the unfolded protein response in prion-related disorders. *Curr. Mol. Med.* **6**, 37–43
4. Puig, B., Altmeppen, H., and Glatzel, M. (2014) The GPI-anchoring of PrP: Implications in sorting and pathogenesis. *Prion*. **8**, 1–8
5. Yedidia, Y., Horonchik, L., Tzaban, S., Yanai, A., and Taraboulos, A. (2001) Proteasomes and ubiquitin are involved in the turnover of the wild-type prion protein. *EMBO J.* **20**, 5383–5391
6. Ma, J., and Lindquist, S. (2001) Wild-type PrP and a mutant associated with prion disease are subject to retrograde transport and proteasome degradation. *Proc. Natl. Acad. Sci. U. S. A.* **98**, 14955–14960
7. Vey, M., Pilkuhn, S., Wille, H., Nixon, R., DeArmond, S. J., Smart, E. J., Anderson, R. G., Taraboulos, A., and Prusiner, S. B. (1996) Subcellular colocalization of the cellular and scrapie prion proteins in caveolae-like membranous domains. *Proc. Natl. Acad. Sci. U. S. A.* **93**, 14945–14949
8. Hetz, C., Lee, A.-H., Gonzalez-Romero, D., Thielen, P., Castilla, J., Soto, C., and Glimcher, L. H. (2008) Unfolded protein response transcription factor XBP-1 does not influence prion replication or pathogenesis. *Proc. Natl. Acad. Sci. U. S. A.* **105**, 757–762
9. Hetz, C., Russelakis-Carneiro, M., Maundrell, K., Castilla, J., and Soto, C. (2003) Caspase-12 and endoplasmic reticulum stress mediate neurotoxicity of pathological prion protein. *EMBO J.* **22**, 5435–5445

10. Hetz, C., Russelakis-Carneiro, M., Wälchli, S., Carboni, S., Vial-Knecht, E., Maundrell, K., Castilla, J., and Soto, C. (2005) The disulfide isomerase Grp58 is a protective factor against prion neurotoxicity. *J. Neurosci.* **25**, 2793–2802

11. Moreno, J. A., Halliday, M., Molloy, C., Radford, H., Verity, N., Axten, J. M., Ortori, C. A., Willis, A. E., Fischer, P. M., Barrett, D. A., and Mallucci, G. R. (2013) Oral treatment targeting the unfolded protein response prevents neurodegeneration and clinical disease in prion-infected mice. *Sci. Transl. Med.* **5**, 206ra138

12. Moreno, J. a, Radford, H., Peretti, D., Steinert, J. R., Verity, N., Martin, M. G., Halliday, M., Morgan, J., Dinsdale, D., Ortori, C. a, Barrett, D. a, Tsaytler, P., Bertolotti, A., Willis, A. E., Bushell, M., and Mallucci, G. R. (2012) Sustained translational repression by eIF2α-P mediates prion neurodegeneration. *Nature.* **485**, 507–11

13. Rane, N. S., Kang, S. W., Chakrabarti, O., Feigenbaum, L., and Hegde, R. S. (2008) Reduced Translocation of Nascent Prion Protein During ER Stress Contributes to Neurodegeneration. *Dev. Cell.* **15**, 359–370

14. Steele, A. D., Hetz, C., Yi, C. H., Jackson, W. S., Borkowski, A. W., Yuan, J., Wollmann, R. H., and Lindquist, S. (2007) Prion pathogenesis is independent of caspase-12. *Prion.* **1**, 243–247

15. Torres, M., Castillo, K., Armisén, R., Stutzin, A., Soto, C., and Hetz, C. (2010) Prion Protein Misfolding Affects Calcium Homeostasis and Sensitizes Cells to Endoplasmic Reticulum Stress. *PLoS One.* **5**, e15658

16. Xu, K., and Zhu, X.-P. (2012) Endoplasmic reticulum stress and prion diseases. *Rev. Neurosci.* **23**, 79-84

17. Quaglio, E., Restelli, E., Garofoli, A., Dossena, S., de Luigi, A., Tagliavacca, L., Imperiale, D., Migheli, A., Salmona, M., Sitia, R., Forloni, G., and Chiesa, R. (2011) Expression of mutant or cytosolic PrP in transgenic mice and cells is not associated with endoplasmic reticulum stress or proteasome dysfunction. *PLoS One.* **6**, e19339

18. Wang, S. Bin, Shi, Q., Xu, Y., Xie, W. L., Zhang, J., Tian, C., Guo, Y., Wang, K., Zhang, B. Y., Chen, C., Gao, C., and Dong, X. P. (2012) Protein disulfide isomerase regulates endoplasmic reticulum stress and the apoptotic process during prion infection and PrP mutant-induced cytotoxicity. *PLoS One.* **7**, e38221

19. Wang, X., Shi, Q., Xu, K., Gao, C., Chen, C., Li, X. L., Wang, G. R., Tian, C., Han, J., and Dong, X. P. (2011) Familial CJD associated PrP mutants within transmembrane region induced CTM-PrP retention in ER and Triggered apoptosis by ER stress in SH-SY5Y cells. *PLoS One.* **6**, e14602

20. Hetz, C. (2012) The unfolded protein response: controlling cell fate decisions under ER stress and beyond. *Nat. Rev. Mol. Cell Biol.* **13**, 89–102

21. Walter, P., and Ron, D. (2011) The unfolded protein response: from stress pathway to homeostatic regulation. *Science.* **334**, 1081–6

22. Hetz, C., Chevet, E., and Oakes, S. A. (2015) Proteostasis control by the unfolded protein response. *Nat. Cell Biol.* **17**, 1–10

23. Kang, S. W., Rane, N. S., Kim, S. J., Garrison, J. L., Taunton, J., and Hegde, R. S. (2006) Substrate-Specific Translocational Attenuation during ER Stress Defines a Pre-Emptive Quality Control Pathway. *Cell.* **127**, 999–1013

24. Orsi, A., Fioriti, L., Chiesa, R., and Sitia, R. (2006) Conditions of endoplasmic reticulum stress favor the accumulation of cytosolic prion protein. *J. Biol. Chem.* **281**, 30431–30438

25. Nunziante, M., Ackermann, K., Dietrich, K., Wolf, H., Gädtke, L., Gilch, S., Vorberg, I., Groschup, M., and Schätzl, H. M. (2011) Proteasomal dysfunction and endoplasmic reticulum stress enhance trafficking of prion protein aggregates through the secretory pathway and increase accumulation of pathologic prion protein. *J. Biol. Chem.* **286**, 33942–33953

26. Hetz, C., Castilla, J., and Soto, C. (2007) Perturbation of endoplasmic reticulum homeostasis facilitates prion replication. *J. Biol. Chem.* **282**, 12725–12733

27. Hetz, C., and Mollereau, B. (2014) Disturbance of endoplasmic reticulum proteostasis in neurodegenerative diseases. *Nat. Rev. Neurosci.* **15**, 233–49

28. Yoo, B. C., Krapfenbauer, K., Cairns, N., Belay, G., Bajo, M., and Lubec, G. (2002) Overexpressed protein disulfide isomerase in brains of patients with sporadic Creutzfeldt-Jakob disease. *Neurosci. Lett.* **334**, 196–200

29. Feige, M. J., and Hendershot, L. M. (2011) Disulfide bonds in ER protein folding and homeostasis. *Curr. Opin. Cell Biol.* **23**, 167–75

30. Andreu, C. I., Woehlbier, U., Torres, M., and Hetz, C. (2012) Protein disulfide isomerases in neurodegeneration: from disease mechanisms to biomedical applications. *FEBS Lett.* **586**, 2826–34

31. Jessop, C. E., Tavender, T. J., Watkins, R. H., Chambers, J. E., and Bulleid, N. J. (2009) Substrate specificity of the oxidoreductase ERp57 is determined primarily by its interaction with calnexin and calreticulin. *J. Biol. Chem.* **284**, 2194–2202

32. Coe, H., and Michalak, M. (2010) ERp57, a multifunctional endoplasmic reticulum resident oxidoreductase. *Int. J. Biochem. Cell Biol.* **42**, 796–799

33. Garbi, N., Tanaka, S., Momburg, F., and Hämmerling, G. J. (2006) Impaired assembly of the major histocompatibility complex class I peptide-loading complex in mice deficient in the oxidoreductase ERp57. *Nat. Immunol.* **7**, 93–102

34. Coe, H., Jung, J., Groenendyk, J., Prins, D., and Michalak, M. (2010) ERp57 modulates STAT3 signaling from the lumen of the endoplasmic reticulum. *J. Biol. Chem.* **285**, 6725–6738

35. Jessop, C. E., Chakravarthi, S., Garbi, N., Hämmerling, G. J., Lovell, S., and Bulleid, N. J. (2007) ERp57 is essential for efficient folding of glycoproteins sharing common structural domains. *EMBO J.* **26**, 28–40

36. Solda, T., Garbi, N., Hämmerling, G. J., and Molinari, M. (2006) Consequences of ERp57 deletion on oxidative folding of obligate and facultative clients of the calnexin cycle. *J. Biol. Chem.* **281**, 6219–6226

37. Garbi, N., Hämmerling, G., and Tanaka, S. (2007) Interaction of ERp57 and tapasin in the generation of MHC class I-peptide complexes. *Curr. Opin. Immunol.* **19**, 99–105

38. Wearsch, P. A., and Cresswell, P. (2007) Selective loading of high-affinity peptides onto major histocompatibility complex class I molecules by the tapasin-ERp57 heterodimer. *Nat. Immunol.* **8**, 873–881

39. Peaper, D. R., and Cresswell, P. (2008) The redox activity of ERp57 is not essential for its functions in MHC class I peptide loading. *Proc. Natl. Acad. Sci. U. S. A.* **105**, 10477–10482

40. Turano, C., Gaucci, E., Grillo, C., and Chichiarelli, S. (2011) ERp57/GRP58: A protein with multiple functions. *Cell. Mol. Biol. Lett.* **16**, 539–563

41. Li, Y., and Camacho, P. (2004) Ca2+-dependent redox modulation of SERCA 2b by ERp57. *J. Cell Biol.* **164**, 35–46

42. Hoffstrom, B. G., Kaplan, A., Letso, R., Schmid, R. S., Turmel, G. J., Lo, D. C., and Stockwell, B. R. (2010) Inhibitors of protein disulfide isomerase suppress apoptosis induced by misfolded proteins. *Nat. Chem. Biol.* **6**, 900–6

43. Watts, J. C., Huo, H., Bai, Y., Ehsani, S., Jeon, A. H. W., Shi, T., Daude, N., Lau, A., Young, R., Xu, L., Carlson, G. A., Williams, D., Westaway, D., and Schmitt-Ulms, G. (2009) Interactome analyses identify ties of PrP and its mammalian paralogs to oligomannosidic N-glycans and endoplasmic reticulum-derived chaperones. *PLoS Pathog.* **5**, e1000608

44. Capellari, S., Zaidi, S. I. A., Urig, C. B., Perry, G., Smith, M. A., and Petersen, R. B. (1999) Prion protein glycosylation is sensitive to redox change. *J. Biol. Chem.* **274**, 34846–34850

45. Lucassen, R., Nishina, K., and Supattapone, S. (2003) In vitro amplification of protease-resistant prion protein requires free sulfhydryl groups. *Biochemistry*. **42**, 4127–4135

46. Tompa, P., Tusnády, G. E., Friedrich, P., and Simon, I. (2002) The role of dimerization in prion replication. *Biophys. J.* **82**, 1711–1718

47. Welker, E., Wedemeyer, W. J., and Scheraga, H. A. (2001) A role for intermolecular disulfide bonds in prion diseases? *Proc. Natl. Acad. Sci. U. S. A.* **98**, 4334–4336

48. Yanai, A., Meiner, Z., Gahali, I., Gabizon, R., and Taraboulos, A. (1999) Subcellular trafficking abnormalities of a prion protein with a disrupted disulfide loop. *FEBS Lett.* **460**, 11–16

49. Ma, J., and Lindquist, S. (1999) De novo generation of a PrPSc-like conformation in living cells. *Nat. Cell Biol.* **1**, 358–361

50. Ivanova, L., Barmada, S., Kummer, T., and Harris, D. A. (2001) Mutant Prion Proteins Are Partially Retained in the Endoplasmic Reticulum. *J. Biol. Chem.* **276**, 42409–42421

51. Burgos, P. V, Mardones, G. A., Rojas, A. L., DaSilva, L. L. P., Prabhu, Y., Hurley, J. H., and Bonifacino, J. S. (2010) Sorting of the Alzheimer's disease amyloid precursor protein mediated by the AP-4 complex. *Dev. Cell*. **18**, 425–436

52. Jessop, C. E., Watkins, R. H., Simmons, J. J., Tasab, M., and Bulleid, N. J. (2009) Protein disulphide isomerase family members show distinct substrate specificity: P5 is targeted to BiP client proteins. *J. Cell Sci.* **122**, 4287–4295

53. Moffat, J., Grueneberg, D. A., Yang, X., Kim, S. Y., Kloepfer, A. M., Hinkle, G., Piqani, B., Eisenhaure, T. M., Luo, B., Grenier, J. K., Carpenter, A. E., Foo, S. Y., Stewart, S. A., Stockwell, B. R., Hacohen, N., Hahn, W. C., Lander, E. S., Sabatini, D. M., and Root, D. E. (2006) A Lentiviral RNAi Library for Human and Mouse Genes Applied to an Arrayed Viral High-Content Screen. *Cell*. **124**, 1283–1298

54. Hetz, C., Thielen, P., Matus, S., Nassif, M., Court, F., Kiffin, R., Martinez, G., Cuervo, A. M., Brown, R. H., and Glimcher, L. H. (2009) XBP-1 deficiency in the nervous system protects against amyotrophic lateral sclerosis by increasing autophagy. *Genes Dev.* **23**, 2294–306

55. Lisbona, F., Rojas-Rivera, D., Thielen, P., Zamorano, S., Todd, D., Martinon, F., Glavic, A., Kress, C., Lin, J. H., Walter, P., Reed, J. C., Glimcher, L. H., and Hetz, C. (2009) BAX inhibitor-1 is a negative regulator of the ER stress sensor IRE1alpha. *Mol. Cell*. **33**, 679–91

56. Rodriguez, D. a, Zamorano, S., Lisbona, F., Rojas-Rivera, D., Urra, H., Cubillos-Ruiz, J. R., Armisen, R., Henriquez, D. R., Cheng, E. H., Letek, M., Vaisar, T., Irrazabal, T., Gonzalez-Billault, C., Letai, A., Pimentel-Muiños, F. X., Kroemer, G., and Hetz, C. (2012) BH3-only proteins are part of a regulatory network that control the sustained signalling of the unfolded protein response sensor IRE1α. *EMBO J.* **31**, 2322–35

57. Castillo, V., Oñate, M., Woehlbier, U., Rozas, P., Andreu, C., Medinas, D. B., Valdes, P., Osorio, F., Vidal, R. L., Kerr, B., Court, F. A., and Hetz, C. (2015) Functional role of the disulfide isomerase ERp57 in axonal regeneration. *PLoS One. in press*

58. Borchelt, D. R., Davis, J., Fischer, M., Lee, M. K., Slunt, H. H., Ratovitsky, T., Regard, J., Copeland, N. G., Jenkins, N. A., Sisodia, S. S., and Price, D. L. (1996) A vector for expressing foreign genes in the brains and hearts of transgenic mice. *Genet. Anal. - Biomol. Eng.* **13**, 159–163

59. Rojas-Rivera, D., Armisén, R., Colombo, a, Martínez, G., Eguiguren, a L., Díaz, a, Kiviluoto, S., Rodríguez, D., Patron, M., Rizzuto, R., Bultynck, G., Concha, M. L., Sierralta, J., Stutzin, a, and Hetz, C. (2012) TMBIM3/GRINA is a novel unfolded protein response (UPR) target gene that controls apoptosis through the modulation of ER calcium homeostasis. *Cell Death Differ.* **19**, 1013–26

60. Hetz, C., Bernasconi, P., Fisher, J., Lee, A.-H., Bassik, M. C., Antonsson, B., Brandt, G. S., Iwakoshi, N. N., Schinzel, A., Glimcher, L. H., and Korsmeyer, S. J. (2006) Proapoptotic BAX and BAK modulate the unfolded protein response by a direct interaction with IRE1alpha. *Science*. **312**, 572–576

61. Stewart, R. S., Piccardo, P., Ghetti, B., and Harris, D. A. (2005) Neurodegenerative illness in transgenic mice expressing a transmembrane form of the prion protein. *J. Neurosci.* **25**, 3469–3477

62. Chiesa, R., Piccardo, P., Ghetti, B., and Harris, D. A. (1998) Neurological illness in transgenic mice expressing a prion protein with an insertional mutation. *Neuron*. **21**, 1339–1351

63. Dossena, S., Imeri, L., Mangieri, M., Garofoli, A., Ferrari, L., Senatore, A., Restelli, E., Balducci, C., Fiordaliso, F., Salio, M., Bianchi, S., Fioriti, L., Morbin, M., Pincherle, A., Marcon, G., Villani, F., Carli, M., Tagliavini, F., Forloni, G., and Chiesa, R. (2008) Mutant Prion Protein Expression Causes Motor and Memory Deficits and Abnormal Sleep Patterns in a Transgenic Mouse Model. *Neuron*. **60**, 598–609

64. Drisaldi, B., Stewart, R. S., Adles, C., Stewart, L. R., Quaglio, E., Biasini, E., Fioriti, L., Chiesa, R., and Harris, D. A. (2003) Mutant PrP is delayed in its exit from the endoplasmic reticulum, but neither wild-type nor mutant PrP undergoes retrotranslocation prior to proteasomal degradation. *J. Biol. Chem.* **278**, 21732–21743

65. Stewart, R. S., Drisaldi, B., and Harris, D. A. (2001) A transmembrane form of the prion protein contains an uncleaved signal peptide and is retained in the endoplasmic Reticulum. *Mol. Biol. Cell*. **12**, 881–889

66. Ashok, A., and Hegde, R. S. (2008) Retrotranslocation of prion proteins from the endoplasmic reticulum by preventing GPI signal transamidation. *Mol. Biol. Cell*. **19**, 3463–3476

67. Satpute-Krishnan, P., Ajinkya, M., Bhat, S., Itakura, E., Hegde, R. S., and Lippincott-Schwartz, J. (2014) ER stress-induced clearance of misfolded GPI-anchored proteins via the secretory pathway. *Cell*. **158**, 522–533

68. Moya, K. L., Hässig, R., Breen, K. C., Volland, H., and Di Giamberardino, L. (2005) Axonal transport of the cellular prion protein is increased during axon regeneration. *J. Neurochem.* **92**, 1044–1053

69. Bremer, J., Baumann, F., Tiberi, C., Wessig, C., Fischer, H., Schwarz, P., Steele, A. D., Toyka, K. V, Nave, K.-A., Weis, J., and Aguzzi, A. (2010) Axonal prion protein is required for peripheral myelin maintenance. *Nat. Neurosci.* **13**, 310–318

70. Uehara, T., Nakamura, T., Yao, D., Shi, Z.-Q., Gu, Z., Ma, Y., Masliah, E., Nomura, Y., and Lipton, S. A. (2006) S-nitrosylated protein-disulphide isomerase links protein misfolding to neurodegeneration. *Nature*. **441**, 513–7

ABBREVIATIONS

The abbreviations used are: PrP, prion protein; PrP^C, wild-type PrP; PrP^{RES}, protease-resistant PrP; PrDs, Prion-related Disorders; PDI, protein disulfide isomerase; CNS, Central Nervous System; CJD, Creutzfeldt-Jacob Diseases; FFI, Fatal Familial Insomnia; ALS, Amyotrophic Lateral Sclerosis; CNX, Calnexin; CRT, Calreticulin; MEFs, Murine Embryonic Fibroblast; ER, Endoplasmic Reticulum; UPR, unfolded protein response; ERAD, ER-associated degradation; PK, proteinase K; RESET, rapid ER stress-induced export; APP, amyloid precursor protein; Tm, tunicamycin; Thp, thapsigargin; Bref A, brefeldin A; CHX, cycloheximide; TBS, Tris-buffered saline; PBS, phosphate-buffered saline; HBS, HEPES-buffered saline; PFA, paraformaldehyde; BSA, bovine serum albumin.

FIGURE LEGENDS

FIGURE 1. Detection of ERp57 in brain tissue of patients with Creutzfeldt-Jakob disease. (A-D) Brain tissue of three CJD patients and three control subjects were fixed in formalin. After a month of fixation, tissue was embedded in paraffin and cut into 10 μm thick slices. Cerebral tissues were then (A) stained with hematoxylin and eosin (H&E), (B) processed for immunohistochemistry using anti-PrP (3F4) antibody in cortex, or (C) anti-ERp57, and (D) anti-PDIA1, anti-ERp72, anti-KDEL antibodies in cerebellum. Black arrows indicate positive reaction to ERp57 in Purkinje cells. Scale bars represent 50 μm.

FIGURE 2. PrP levels in ERp57-deficient cells. (A) Endogenous levels of PrP in ERp57-deficient (ERp57^{KO}) and wild-type control (ERp57^{WT}) MEFs were evaluated by Western blot (left panel) using the anti-PrP (6D11) antibody. Quantification of three independent experiments (right panel) was performed. Hsp90 levels were monitored as a loading control. **(B)** Detection of endogenous levels of PrP in Neuro2a cells stably knocked down for ERp57. Neuro2a cells stably expressing shRNA against luciferase was used as control (Mock). β-actin was monitored as a loading control. **(C)** ERp57-deficient and wild-type control MEFs were transfected with 3F4-tagged PrP^C or PrP^{D177N} constructs. After 48 h, PrP levels were analyzed by Western blot using the anti-PrP (3F4) antibody. Hsp90 was used as a loading control. **(D)** ERp57-deficient and wild-type control MEFs were transfected with PrP^C-GFP or PrP^{D177N}-GFP constructs. After 48 h, GFP fluorescence was analyzed by flow cytometry. Three independent experiments were performed. **(E)** ERp57-deficient and wild-type MEFs were transfected with a construct encoding GFP-tagged amyloid precursor protein (APP-GFP). After 48 h, cells were analyzed by flow cytometry (left panel) or fluorescence microscopy (right panel). **(F)** Neuro2a cells were transfected with constructs encoding 3F4-tagged PrP^C or its PrDs-related mutants. Transfection with the empty vector was used as control (Mock). After 48 h, protein (upper panel) and mRNA (lower panel) levels of endogenous ERp57 were measured by Western blot and real-time PCR, respectively. **(G)** The level of spliced

XBP1 mRNA were monitored in Neuro2a cells overexpressing PrP^C or its PrDs-related mutants described in (F) using an PstI and RT-PCR based assay (upper panel) or real-time PCR to specifically amplify the spliced variant (lower panel). **(H)** Neuro2a cells were transfected with constructs encoding 3F4-tagged PrP^C or PrP^{D177N} and 48 h later treated with different concentrations of thapsigargin (Thg). After 16 h of treatment, levels of *Erp57* (upper panel) and *Xbp1s* (lower panel) mRNA were measured by real-time PCR. Bars in panels F, G, and H indicate average and standard deviation of three determinations. When indicated, statistical analysis was performed using Student's t-test in panel (A) and one-way ANOVA with Bonferroni post hoc test in panel (D). Mean ± SEM with *p* values: n.s., $p > 0.05$; *, $p \leq 0.05$; **, $p \leq 0.01$; ***, $p \leq 0.001$. Densitometric analyses were performed using Image J.

FIGURE 3. Endogenous PrP levels in NSC34 cells overexpressing ERp57. (A) NSC34 cells were transfected with empty vector (pcDNA3, Mock) or an ERp57 expression vector. After 24 h of transfection, cells were selected with the antibiotic G418 for two weeks. Then, ERp57 and endogenous PrP levels were analyzed by Western blot. β-actin was used as a loading control. **(B)** NSC34 cells were transiently co-transfected with different PrP-GFP constructs (PrP^C-GFP, PrP^{CTM}-GFP, PrP^{D177N}-GFP or PrP^{PG14}-GFP) together with vector encoding for the ER marker KDEL-dsRED (red). Localization of PrP (green) was analyzed by confocal microscopy. The nucleus was stained with Hoechst (blue). **(C)** NSC34 cells stably overexpressing ERp57 were transiently transfected with constructs encoding 3F4-tagged PrP^c and its PrDs-related mutants (PrP^{CTM}, PrP^{D177N}, PrP^{PG14}, and PrP^{E199K}). After 48 h, the steady-state levels of PrP were analyzed by Western blot using the anti-PrP (3F4) antibody. Hsp90 was monitored as a loading control. **(D)** Proteinase K (PK) resistance of PrP^C and PrP^{D177N} was assessed in protein extracts from NSC34 cells transiently co-expressing ERp57 for 48 h by incubation with the indicated amounts of the protease for 30 min at 37°C followed by Western blot analysis.

FIGURE 4. Pulse-chase assays of PrP in ERp57-deficient MEFs. (A) ERp57 deficient (ERp57^{KO}) and wild-type control (ERp57^{WT}) MEFs were transfected with a construct for PrP^C-3F4. After 16 h, a radioactive pulse was conducted with 0.10 mCi of ^{35}S-Promix per plate. The chase of PrP protein was performed from 10 to 180 min. Then cells were lysed and PrP purified by immunoprecipitation using anti-PrP (3F4) antibody. Samples were analyzed in 12% SDS-PAGE gels under thiol reducing (+DTT, upper panel) and non-reducing (-DTT, lower panel) conditions and revealed by autoradiography. White, gray, and black arrowheads indicate di-, mono-, and non-glycosylated forms of PrP, respectively. The asterisk indicate higher molecular weight forms of PrP containing more complex glycosylations. **(B)** Deglycosylation analysis of PrP^C in MEFs after treatment of protein extracts with PNGase F. The different glycosylation states of PrP are identified as in (A). **(C)** Filter-tap analysis of aggregates of endogenous PrP^C in ERp57-deficient and control MEFs under basal conditions. Dot-blot on PVDF membrane followed by Ponceau S staining or Western blot analysis of Hsp90 and PrP were performed as loading controls. Bands were cropped from their original position for the clarity of presentation. All samples were run in the same electrophoresis and detected in the same Western blot. **(D)** Thiol reduction assay using dithiothreitol (DTT) was performed to determine the dependence of PrP^C aggregates on disulfide crosslinks using filter-trap analysis. Dot-blot on PVDF membrane followed by Ponceau S staining used as loading control. **(E)** ERp57-deficient and wild-type MEFs were transfected with constructs for PrP^C-GFP or APP-GFP. After 48 h, cells were treated with 50 μg/ml cycloheximide (CHX) for the indicated time points and fluorescence intensity measured by flow cytometry. The initial fluorescence was normalized to one unit for control cells to monitor relative protein decay over time. Data represents the average and standard error of three independent experiments. Statistical analysis was performed using two-way ANOVA with Bonferroni post hoc test. Mean ± SEM shown; **, *p ≤ 0.01*.

FIGURE 5. Immunoprecipitation of PrP with ERp57 and PDIA1. (A) HEK293T cells were co-transfected with expression vectors for V5-tagged PDIA1, ERp57 or ERp72 together with 3F4-tagged PrP^C. After 48 h, V5-tagged proteins were immunoprecipitated (IP) and eluted with V5 peptide. The possible interaction of PDIs with PrP was analyzed by Western blot using anti-PrP (3F4) and anti-V5 antibodies. Hsp90 was monitored as a loading control. The inputs and elutions (IP: V5) are shown. **(B)** HEK 293T cells were co-transfected with expression vectors for V5-tagged ERp57 together with 3F4-tagged PrP^C or PrP^{D177N}. After 48 h, V5-tagged

16

proteins were immunoprecipitated and eluted with V5 peptide. The possible interaction of ERp57 with PrP was analyzed by Western blot using anti-PrP (3F4) and anti-V5 antibodies. The inputs and elutions (IP: V5) are shown.
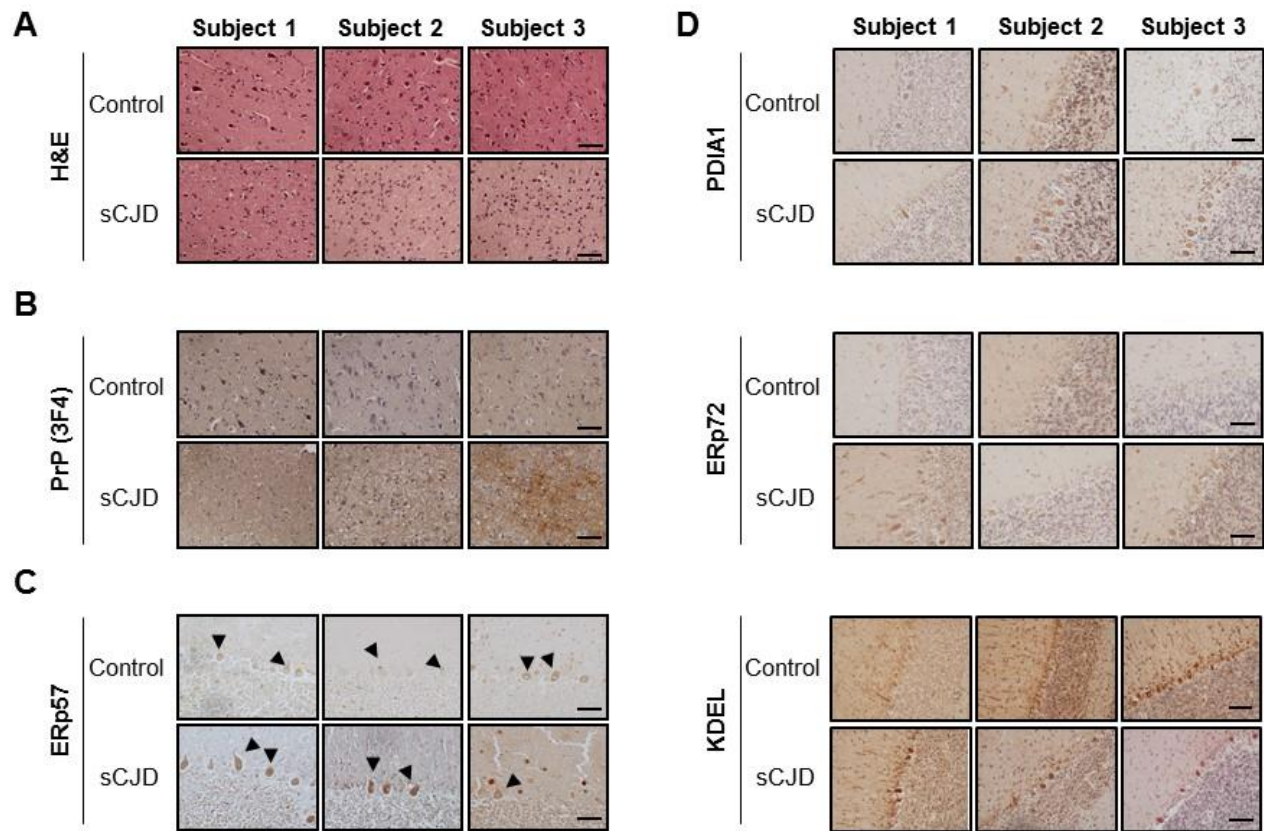
FIGURE 6. Effect of ERp57 expression on ER stress responses. (**A**) ERp57^{WT} and ERp57^{KO} MEFs were treated with the ER stressor tunicamycin (Tm) for 16 h and the levels of indicated ER chaperones and cofactors were measured by Western blot analysis. Hsp90 was employed as a loading control. (**B**) ERp57^{WT} and ERp57^{KO} MEFs were treated or not with tunicamycin (Tm), Thapsigargin (Thg), or Brefeldin A (Bref A), and cell viability assessed 16 h later by the MTT assay. Data represents mean and standard deviation of three measurements. (**C**) NSC34 cells transiently overexpressing V5-tagged ERp57 and Mock control were treated with tunicamycin (Tm) for the indicated time points. ER stress responses were assessed by monitoring the levels of XBP1 spliced (*Xbp1s*) and unspliced (*Xbp1u*) mRNAs, in addition to *Chop* mRNA levels by semi-quantitative RT-PCR. Actin was used as housekeeping control. (**D**) NSC34 cells overexpressing V5-tagged ERp57 and Mock control cells were treated with the ER stressor tunicamycin (Tm) for 16 h and the level of indicated ER folding components measured by Western blot analysis. Hsp90 was employed as a loading control. (**E**) NSC34 cells overexpressing V5-tagged ERp57 and Mock control cells were treated with tunicamycin (Tm) or Thapsigargin (Thg) and cell viability assessed 16 h later by the MTT assay. Data represents mean and standard deviation of three measurements.

FIGURE 7. Endogenous PrP levels on a conditional knockout mice for ERp57. (**A**) *Erp57* floxed animals were crossed with Nestin-Cre transgenic mice to generate CNS-specific knockout and heterozygous animals. The expression levels of ERp57 were evaluated by quantitative real-time PCR in brain cortex tissue of control (ERp57^{WT}), heterozygous (ERp57^{HET}), and homozygous (ERp57^{cKO}) animals. (**B**) ERp57 levels were analyzed in mice of all three genotypes by Western blot of brain cortex, hippocampus, and cerebellum. As a loading control, β-actin levels were determined. (**C**) The level of *PrP* mRNA was determined by real-time PCR in brain cortex of all three genotypes. (**D**) PrP levels were analyzed by Western blot using the anti-PrP (6D11) antibody in cortex tissue of ERp57^{WT} (n = 4), ERp57^{HET} (n = 4), and ERp57^{cKO} (n = 4) animals. ERp57 levels were also determined. β-actin levels were measured as loading control. (**E**) PrP bands were quantified by densitometric analysis using the ImageJ program. Di-glycosylated (left panel), mono-glycosylated (middle panel), and non-glycosylated (right panel) forms of endogenous PrP were quantified and normalized to the loading control. (**F**) Expression levels of *Bip*, *Edem1*, *Pdia1*, and *Chop* mRNA were determined in the cortex of ERp57^{WT}, ERp57^{HET}, and ERp57^{cKO} animals by real-time PCR. All values were normalized to *Actin* mRNA. (**G**) The levels of indicated ER folding components were determined in the cerebellum of ERp57^{WT}, ERp57^{HET}, and ERp57^{cKO} animals by Western blot. β-actin was employed as a loading control. (**H**) Immunofluorescence against NeuN (red) and GFAP (green) to visualize the content of total neurons and astrocytes, respectively, in spinal cord ventral horn (n = 5). Statistical analyses were performed using one-way ANOVA and Bonferroni Multiple Comparison Test. Mean ± SEM shown; *p* values: n.s., $p > 0.05$; *, $p \leq 0.05$; **, $p \leq 0.01$; ***, $p \leq 0.001$.

FIGURE 8. Endogenous PrP levels in animals overexpressing ERp57 in the CNS. A neuronal-specific *Erp57* transgenic mouse was generated using the PrP promoter to drive ERp57-FLAG expression. (**A**) ERp57 protein levels were evaluated in the cerebellum of ERp57 transgenic mice (n = 4) compared to non-transgenic littermates (n = 4) by Western blot analysis. β-actin was used as loading control. (**B**) Immunohistochemistry to ERp57 was also employed to confirm overexpression of the human protein in brain cortex of transgenic mice compared to non-transgenic littermates. Scale bar represents 20 µm. (**C**) Endogenous PrP levels were assessed in the cerebellum of ERp57 transgenic animals (n = 3) compared to non-transgenic littermates (n = 3). Anti-PrP (6D11) antibody was used for Western blot detection. β-actin was used as loading control. Densitometric analysis of PrP levels is shown in the right panel. (**D**) The level of *PrP* mRNA in cerebellum of ERp57 transgenic animals was determined by real-time PCR. (**E**) The levels of *Xbp1s* and *Chop* mRNA were determined by real-time PCR in brain cortex of ERp57 transgenic mice and non-transgenic littermates injected intraperitoneally with 1 µg of the ER stressor tunicamycin (Tm) per gram of body weight or vehicle (150 mM glucose). All values were normalized to actin mRNA (n = 3). Statistical analyses were performed using

17

Student's t-test in panel (C) and one-way ANOVA with Bonferroni Multiple Comparison Test in (E). Mean ± SEM shown; p values: n.s., $p > 0.05$; *, $p \leq 0.05$; **, $p \leq 0.01$; ***, $p \leq 0.001$.
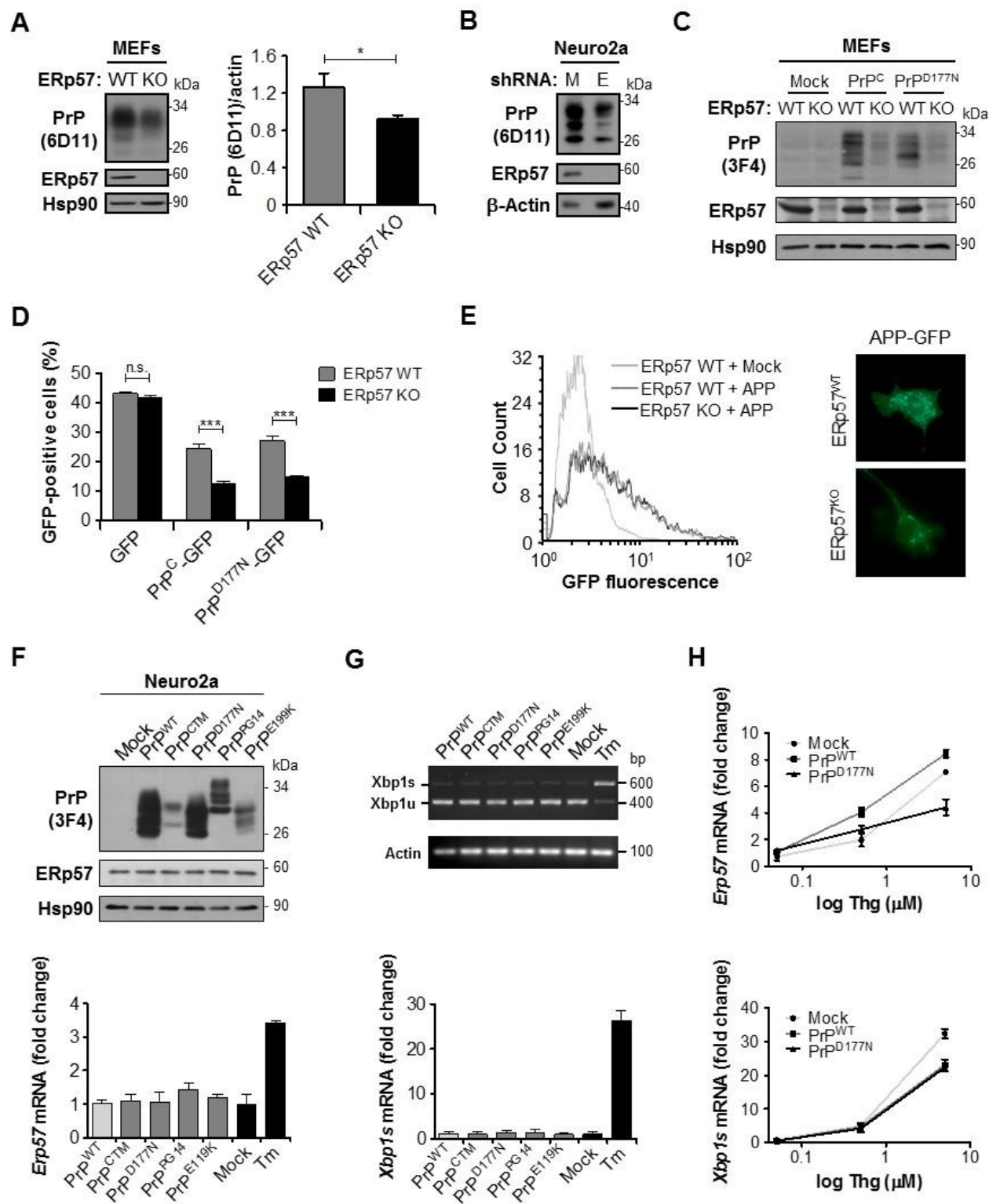
Figure 1

Figure 2

Figure 3
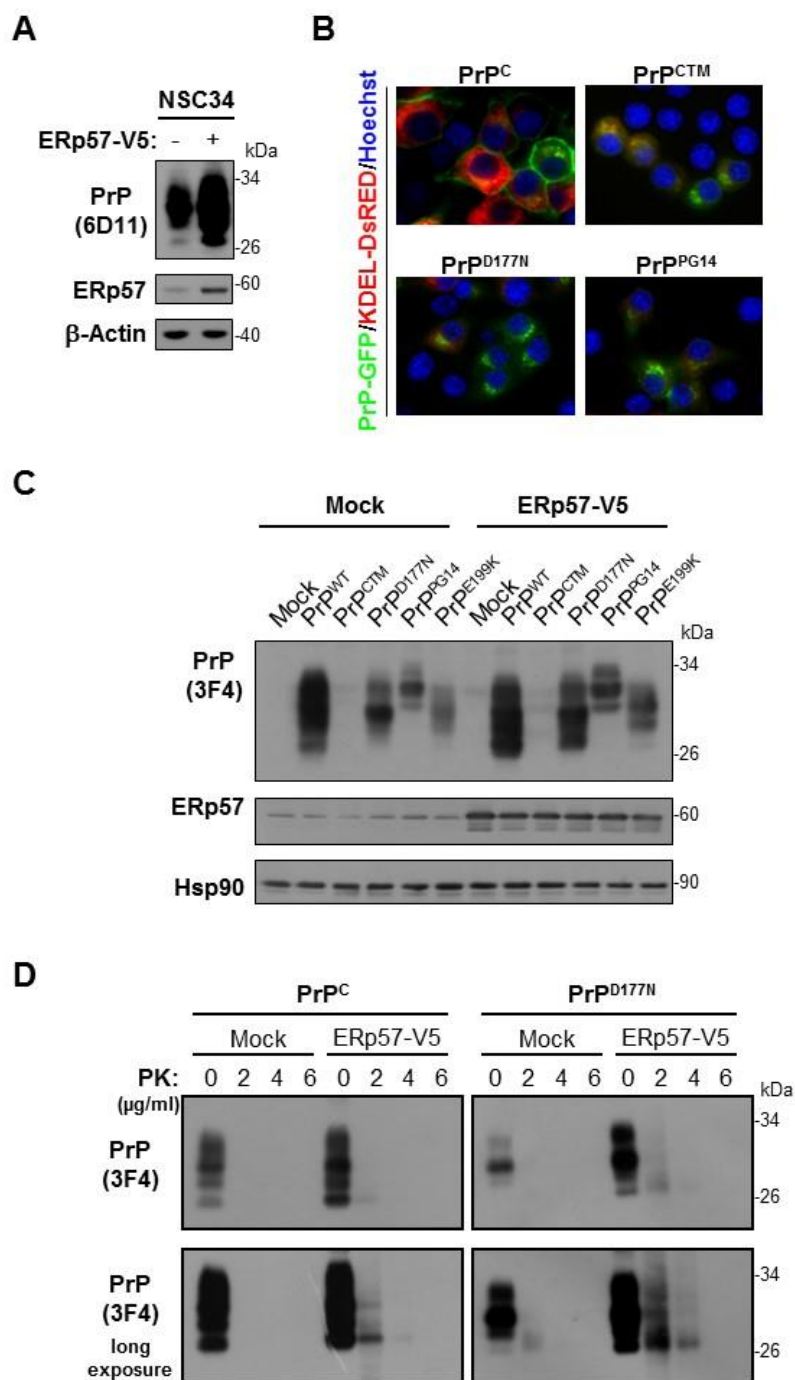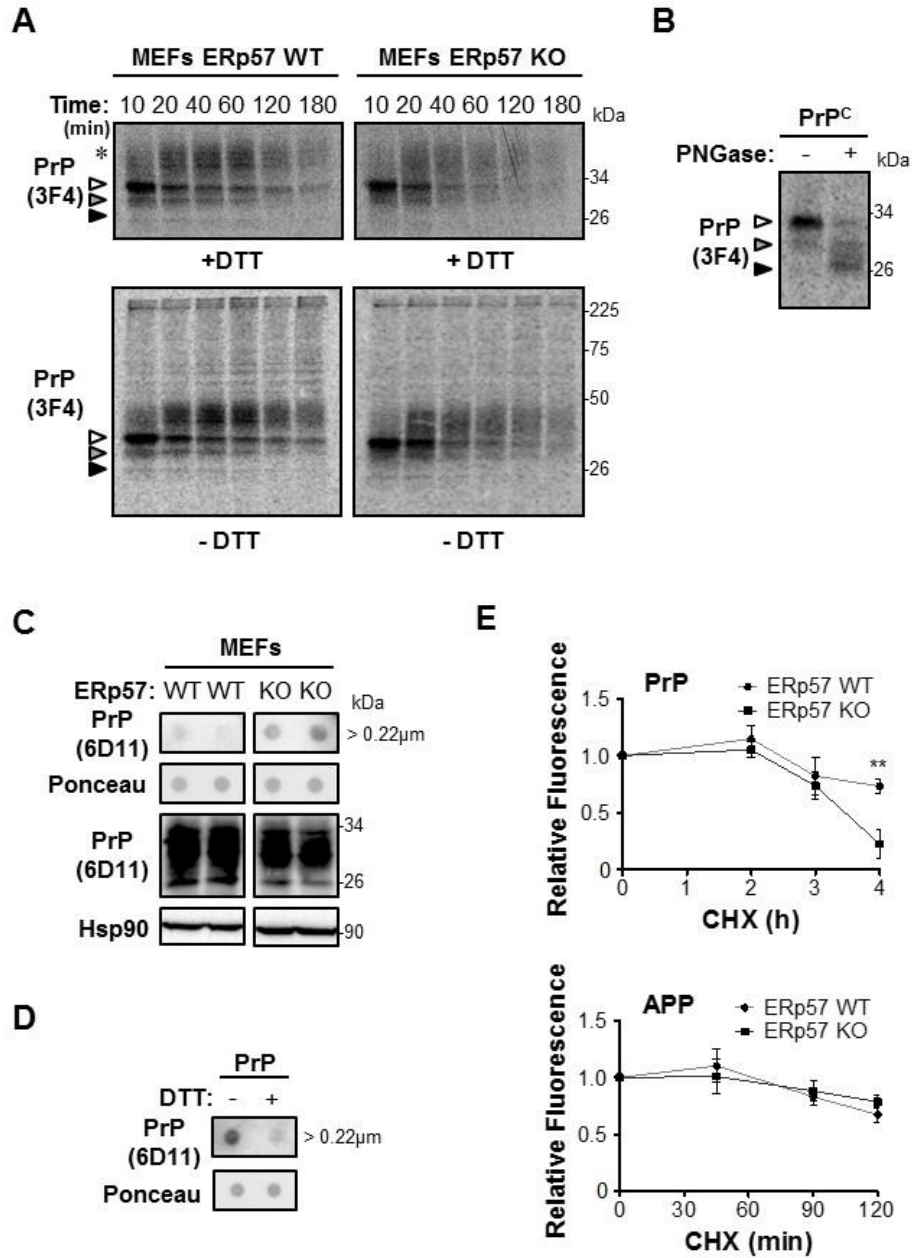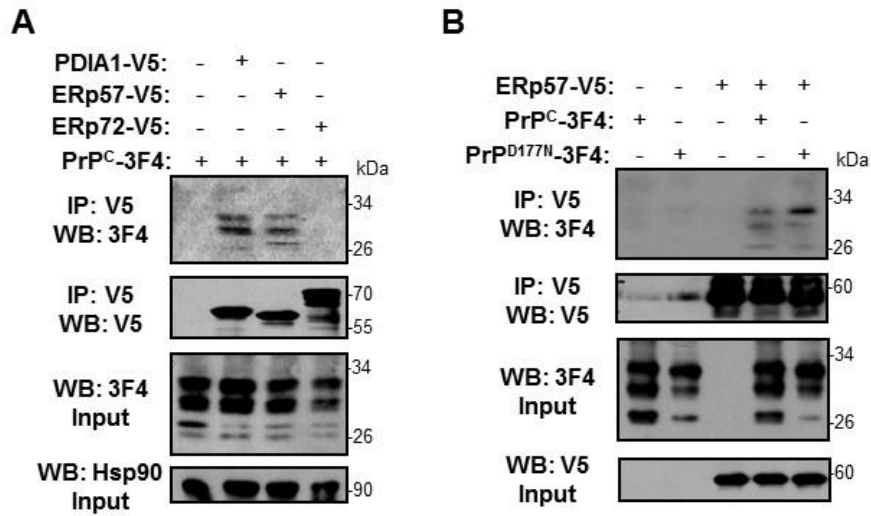
21

Figure 4

A

PDIA1-V5: − + − −
ERp57-V5: − − + −
ERp72-V5: − − − +
PrP^C-3F4: + + + + kDa

IP: V5
WB: 3F4
−34
−26

IP: V5
WB: V5
−70
−55

WB: 3F4
Input
−34
−26

WB: Hsp90
Input
−90

B

ERp57-V5: − − + + +
PrP^C-3F4: + − − + −
PrP^D177N-3F4: − + − − + kDa

IP: V5
WB: 3F4
−34
−26

IP: V5
WB: V5
−60

WB: 3F4
Input
−34
−26

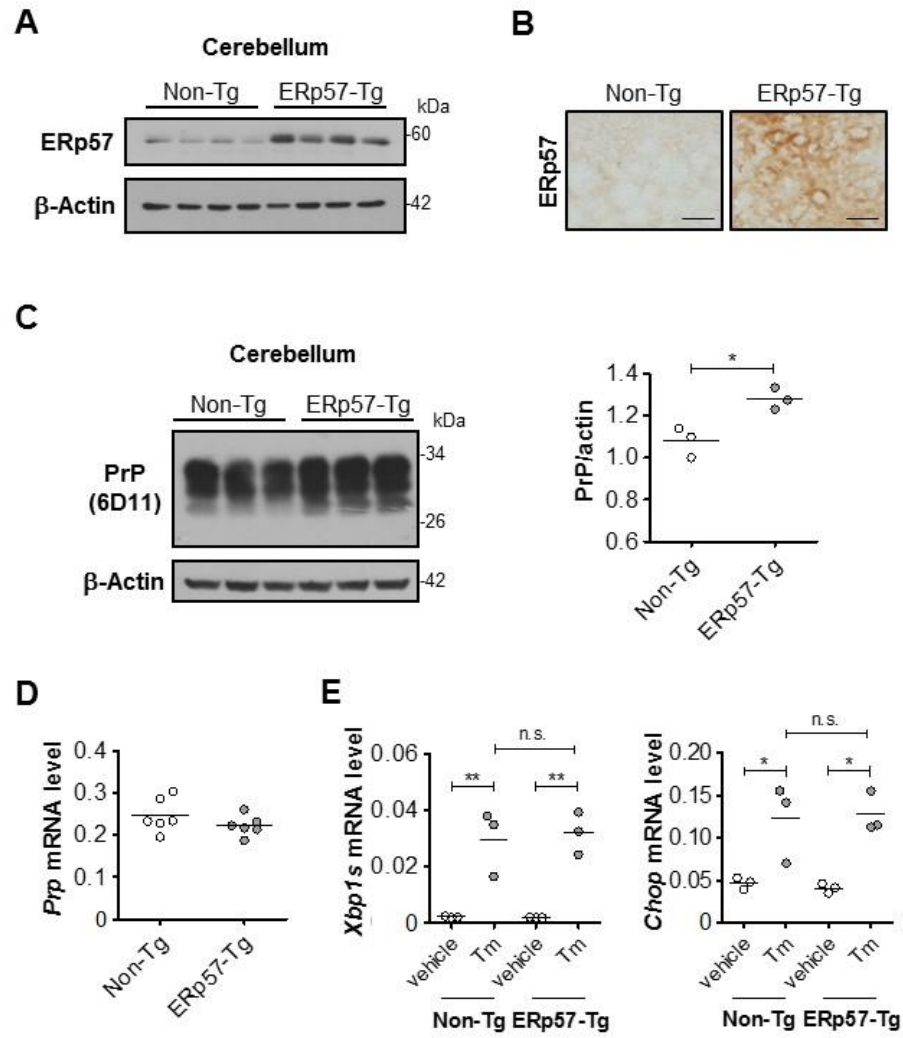WB: V5
Input
−60

Figure 5

23
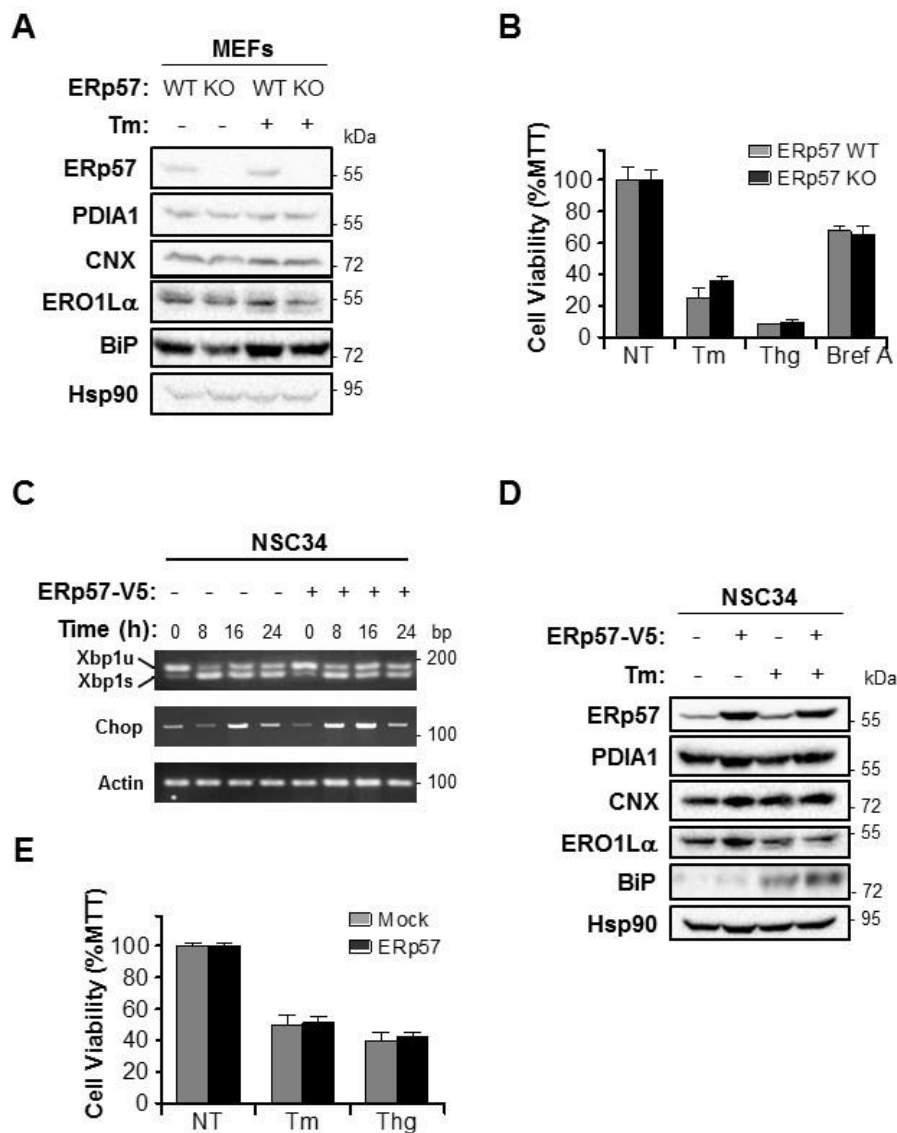
Figure 6

Figure 7

Figure 8

26
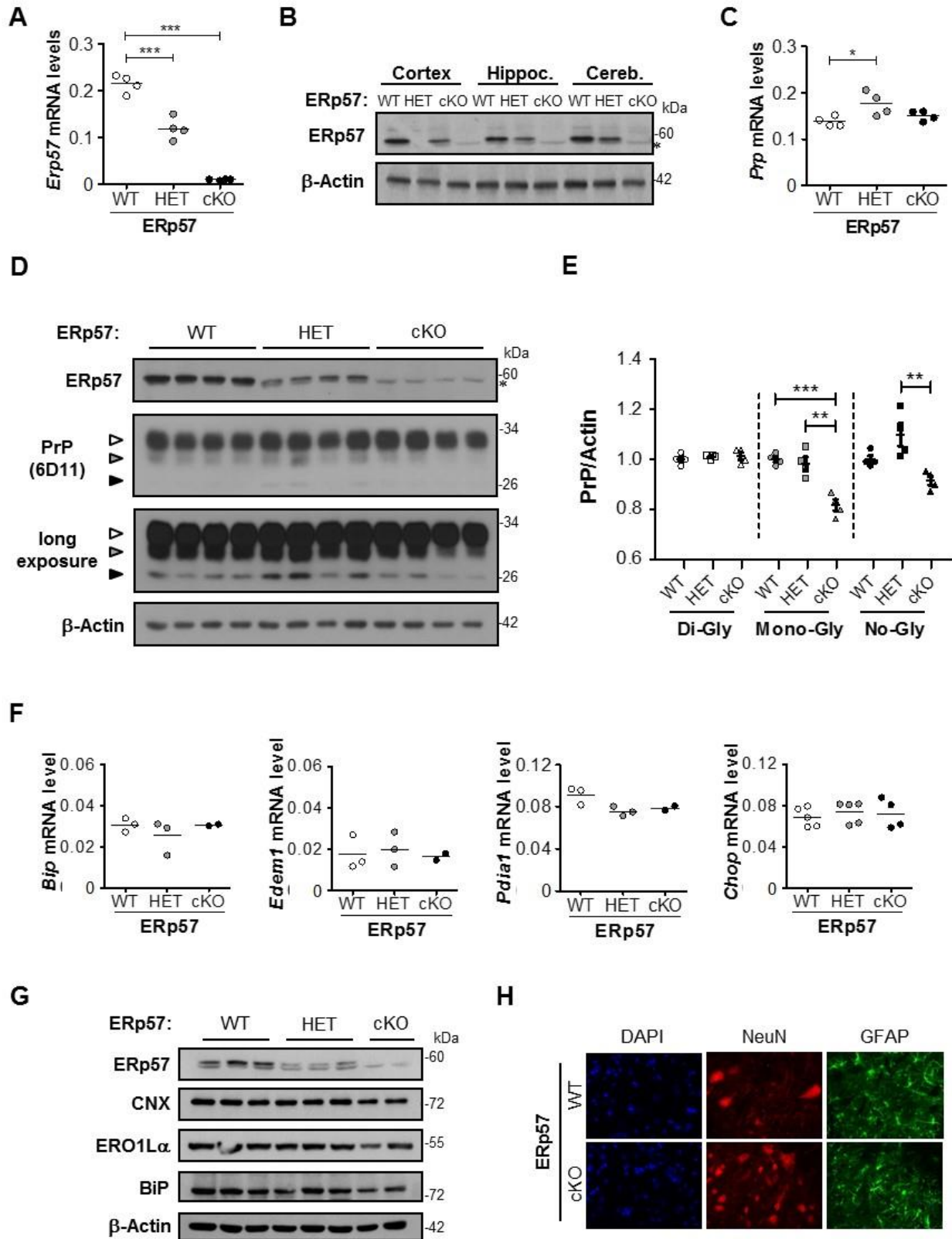
Molecular Bases of Disease:

The Protein Disulfide Isomerase ERp57 Regulates the Steady-State Levels of the Prion Protein

MOLECULAR BASES OF DISEASE

NEUROBIOLOGY

Mauricio Torres, Danilo B. Medinas, José Manuel Matamala, Ute Woehlbier, Víctor Hugo Cornejo, Tatiana Solda, Catherine Andreu, Pablo Rozas, Soledad Matus, Natalia Muñoz, Carmen Vergara, Luis Cartier, Claudio Soto, Maurizio Molinari and Claudio Hetz

Access the most updated version of this article at doi: 10.1074/jbc.M114.635565

Find articles, minireviews, Reflections and Classics on similar topics on the JBC Affinity Sites.

Alerts:
- When this article is cited
- When a correction for this article is posted

Click here to choose from all of JBC's e-mail alerts

This article cites 0 references, 0 of which can be accessed free at
http://www.jbc.org/content/early/2015/07/13/jbc.M114.635565.full.html#ref-list-1